Petroleum Science 20 (2023) 3897–3917

Contents lists available at ScienceDirect

Petroleum Science

journal homepage: www.keaipublishing.com/en/journals/petroleum-science

Original Paper

Numerical simulation study on multiphase flow pattern of hydrate slurry

Xiao-Fang Lv [a, b, *], Feng Chen [a], Jie Zhang [c], Yang Liu [a, **], Qian-Li Ma [a], Hui Du [a], Chuan-Shuo Wang [a], Shi-Dong Zhou [a], Bo-Hui Shi [d], Shang-Fei Song [d], Jing Gong [d]

[a] Jiangsu Key Laboratory of Oil and Gas Storage & Transportation Technology, Changzhou University, Changzhou, 213016, Jiangsu, China
[b] China Petroleum & Chemical Corporation Northwest Oilfield Branch, Petroleum Engineering Technology Research Institute, Urumqi, 830011, Xinjiang, China
[c] Sinopec Shengli Oilfield Company, Dongying, 257001, Shandong, China
[d] National Engineering Laboratory for Pipeline Safety/ MOE Key Laboratory of Petroleum Engineering, China University of Petroleum-Beijing, 102249, Beijing, China

ARTICLE INFO

Article history:
Received 2 February 2023
Received in revised form
7 May 2023
Accepted 8 August 2023
Available online 9 August 2023

Edited by Jia-Jia Fei and Min Li

Keywords:
Hydrate slurry
Numerical simulation
Multiphase flow
Flow field distribution
Flow pattern transition

ABSTRACT

The research on the multiphase flow characteristics of hydrate slurry is the key to implementing the risk prevention and control technology of hydrate slurry in deep-water oil and gas mixed transportation system. This paper established a geometric model based on the high-pressure hydrate slurry experimental loop. The model was used to carry out simulation research on the flow characteristics of gas-liquid-solid three-phase flow. The specific research is as follows: Firstly, the effects of factors such as slurry flow velocity, hydrate particle density, hydrate particle size, and hydrate volume fraction on the stratified smooth flow were specifically studied. Orthogonal test obtained particle size has the most influence on the particle concentration distribution. The slurry flow velocity is gradually increased based on stratified smooth flow. Various flow patterns were observed and their characteristics were analyzed. Secondly, increasing the slurry velocity to 2 m/s could achieve the slurry flow pattern of partial hydrate in the pipeline transition from stratified smooth flow to wavy flow. When the flow rate increases to 3 m/s, a violent wave forms throughout the entire loop. Based on wave flow, as the velocity increased to 4 m/s, and the flow pattern changed to slug flow. When the particle concentration was below 10%, the increase of the concentration would aggravate the slug flow trend; if the particle concentration was above 10%, the increase of the concentration would weaken the slug flow trend, the increase of particle density and liquid viscosity would weaken the tendency of slug flow. The relationship between the pressure drop gradients of several different flow patterns is: slug flow > wave flow > stratified smooth flow.

1. Introduction

Natural gas hydrate is a cage-type ice crystal compound formed by methane, ethane and other gases and water under high pressure and low temperature (Koh et al., 2012; Shi et al., 2021; Sloan and Koh, 2007). Natural gas hydrate is considered to be the source of future fuel due to its abundancy and broad development prospects (Yang et al., 2019; Zhang et al., 2021). However, in the process of production, the growth and accumulation of natural gas hydrates will seriously harm the safe operation of pipelines, as shown in Fig. 1. Gas hydrates have been a major hazard to the flow assurance of subsea transportation system (Sloan et al., 2011).

In the risk prevention and control strategy of natural gas hydrate, the addition of thermodynamic inhibitors to the system is the earliest and most widely used method, which can significantly inhibit the formation of natural gas hydrate (Paz and Netto, 2020; Xu et al., 2021). However, many shortcomings are found such as large dosage, high cost, and environmental pollution. Therefore, in recent years, researchers have proposed a new type of hydrate slurry risk prevention and control technology for the above problems. This technique slows down the formation of hydrates by

* Corresponding author. Jiangsu Key Laboratory of Oil and Gas Storage & Transportation Technology, Changzhou University, Changzhou, 213016, Jiangsu, China.
** Corresponding author.
E-mail address: lvxiaofang5@126.com (X.-F. Lv).

https://doi.org/10.1016/j.petsci.2023.08.008

Fig. 1. Hydrate blocking submarine pipeline.

adding a certain amount of LDHIs (low-dose hydrate inhibitors) such as KHI (kinetics hydrate inhibitors) and AAs (anti-agglomerants) to the system, so that the slurry can carry hydrate particles to flow in the pipeline (Wang et al., 2019). As the key to the implementation of new risk prevention and control technologies, in-depth research were needed on the flow characteristics of hydrate slurry, flow pattern transformation, and blockage mechanism.

Studying the flow characteristics of hydrate slurry is worthwhile to further explore the laws of hydrate particles (such as collision, coalescence, fragmentation, deposition, etc.). These laws can provide a certain theoretical basis for the safe and stable transportation of actual oil and gas pipelines. In terms of experiments, the researchers used the high-pressure experimental loop to study the flow of hydrate slurry. The research contents mainly include the influence of basic parameters (such as slurry flow velocity, hydrate volume fraction, water content, temperature, pressure, polymerization inhibitor, etc.) on slurry viscosity, flow velocity, pressure drop, etc., abundant experimental results had been obtained.

Research (Bai et al., 2015) has shown that the viscosity of hydrate slurry is related to the external environment, and affected by the properties of the slurry and particles. Peng et al. (2012) analyzed the viscosity of hydrate slurries with the help of a U-bend, their results showed that the increase of hydrate volume fraction would significantly intensify the non-Newtonian characteristics of hydrate slurries. Ding et al. (2019) improved and modified the Camargo–Palermo model by considering the volume of unconverted water. The experiments of Sun et al. (2019) showed that the rheology and shear rate of methane hydrate mud were closely related. Empirical Herschel– Bulkley-type equations were developed for the conditions at a low shear rate and a high shear rate, respectively. The flow velocity is critical to ensure that the hydrate slurry flows in a non-sedimented form. Lv et al. (2013) found that if the initial flow velocity is lower than a certain value, the hydrate particles will deposit to form a sedimentary bed. This critical value is defined as “critical suspension flow velocity”. Gong et al. (2020) found in the hydrate slurry rheological experiments, when the slurry flow velocity was increased, the hydrate particles in the transparent pipe section were changed from a sedimentary state to a moving bed in a suspended dispersion state. The hydrate volume fraction affects the slurry flow characteristics and has a critical value. Shen et al. (2018) studied the flow of methane hydrate in the velocity range of 0.62–3.84 m/s, they found that turbulent flow was easy to occur in the region with low hydrate volume fraction and high flow velocity. As the hydrate volume fraction increased, the turbulent flow was transformed into a laminar flow. All rheological parameters were regressed as a function of hydrate concentration and shear rate according to the empirical Herschel–Bulkley-type equations established by Sun et al. (2019). The deposition of hydrate in the pipeline can lead to an increase in the pressure drop in the pipeline. Joshi et al. (2013) found in the multiphase flow experiment of hydrate slurry, a small amount of hydrate particles would promote the development of hydrate slurry at the boundary of the stratified flow and the slug flow to the slug flow. Gong et al. (2020) found that the increase of hydrate particles concentration would cause transition the slurry flow pattern from stratified flow to slug flow, annual flow, and other flow patterns. Ding et al. (2017) conducted a three-phase flow experiment of hydrate slurry with a high-pressure loop. They concluded that the aggregation trend of hydrate particles in the multiphase system was faster and more intense than that in the single-phase system.

At present, the research on the multiphase flow characteristics of natural gas hydrate slurry is mostly based on the high-pressure hydrate experimental loop (Lv et al., 2019; Stoporev et al., 2018). However, the generation conditions of the hydrate slurry in the experimental loop were relatively narrow, which cannot cover the harsh operating conditions. The flow pattern of the slurry was not easy to observe. In view of the above deficiencies, scholars (Song et al., 2020; Umuteme et al., 2022) used FLUENT numerical simulation software to fully grasp the flow characteristics of the hydrate slurry under the flow system. Zhong et al. (2021) studied the flow characteristics of R11 hydrate slurry in curved pipes with an inner diameter of 4.52 cm. They also investigated the effects of hydrate particle density and average particle size on the pipeline pressure drop gradient and hydrate particle volume fraction distribution. Wang's team (Wang et al., 2010) developed a hydrate aggregation model. Song et al. (2018) introduced the equilibrium equation into a dynamic model of hydrate agglomeration and fragmentation, drawing conclusions. The particle size distribution of particles gradually follows a lognormal distribution during agglomeration and crushing. They also analyzed the effect of flow rate and hydration volume fraction on the agglomeration process, pointing out that the greater the particle diameter and volume fraction, the more severe the hydrate deposition in the tube. Duan et al. (2021) used FLUENT and EDEM to establish a three-dimensional model of a solid-liquid pipeline containing hydrate particles and obtained the adhesion law of hydrate particles to the pipe wall. However, most of the simulation studies of hydrate slurry under flow systems were based on a single short straight tube or a single 90° elbow modeling. Only a few scholars had established a complete experimental loop model combining straight pipes with curved pipes to analyze the flow field distribution in the changing flow field, slurry flow characteristics, flow pattern transformation, particle merger, deposition, etc. In addition, the analysis of the flow characteristics of hydrate slurry under the flow system was mostly based on the solid-liquid two-phase flow. Few scholars had explored the changes in the flow pattern, flow state, and flow characteristics of the gas slurry from the perspective of gas-liquid-solid three phases to more accurately approach the actual situation of the slurry in the mixed pipeline and improve the scientifically and accuracy of the simulation.

In view of this, a geometric model was established with the help of a high-pressure natural gas hydrate slurry experimental loop, and the model was verified according to the experimental data. The multiphase flow model in FLUENT was used to simulate and analyze the multiphase flow characteristics of hydrate slurry. This paper studied the key factors affecting the flow characteristics of hydrate multiphase flow, flow pattern, flow pattern transformation, as well as particle microscopic characteristics. In this paper, the flow field distribution, flow pattern characteristics, flow pattern transition characteristics, transition mechanism and blocking mechanism of hydrate slurry multiphase flow were analyzed. Finally, this paper proposed an effective scheme for preventing hydrate blockage pipeline under the pipeline transmission system.

Through the simulation and flow characteristics in this paper, this paper strives to qualitatively and quantitatively describe the influence of key parameters on slurry flow and particle deposition characteristics, summarize the multiphase flow law of hydrate slurry under the flow system. It is hoped that the obtained law can be used to reasonably predict the risk reduction of pipeline blockage in the actual oil and gas mixed transportation system.

2. Numerical simulation method

2.1. Geometric model

The geometric model is based on the high-pressure hydrate experimental loop. The schematic diagram of the model is shown in Fig. 2 (Shi et al., 2016), the inner diameter of the tube of the established geometric model is 0.0254 m, a straight pipe section connects entrance and outlet, it is 5 m and much greater than 50 D, which can effectively eliminate the inlet effect and make the hydrate slurry reach a state of sufficient turbulence. The curved section composes of two circular arcs, the angles are 249° and 69°, the radius of curvature is 0.7 m, the lengths are 3.042 and 0.843 m, and the total length of the ring pipe is 13.885 m.

In this paper, the geometry model was meshed with the help of ICEM using O-shaped slicing in a structured mesh, and the mesh size was determined to be 1 mm according to the minimum feature size, as shown in Fig. 3, which was the meshing of the roundabout entrance, the straight pipe section, and the elbow segment. The minimum mesh quality was greater than 0.7 and most of the meshes were mainly concentrated above 0.85. Regarding the verification of grid independence, this paper verified the volume fraction distribution of hydrate particles at 3.8 m from the inlet, as shown in Fig. 4. In this paper, the number of grids in 1094338 was still selected for iterative calculation. For details, please refer to our previous research (Lv et al., 2022).

2.2. Governing equations

The three-phase flow of gas-liquid-solid hydrate slurry is simulated by VOF model. The continuity equation, volume fraction continuity equation, and momentum equation for each phase of the hydrate slurry are listed in Eqs. (1)–(7).

$$\frac{\partial \rho}{\partial t} + \nabla \cdot (\rho v) = 0 \tag{1}$$

$$\frac{\partial \alpha_i}{\partial t} + v \cdot (\alpha_i) = 0 \tag{2}$$

$$\frac{\partial (\rho v)}{\partial t} + \nabla \cdot (\rho v v) = -\nabla p + \nabla \cdot \left[\mu\left(\nabla v + \nabla v^T\right)\right] + \rho g + F \tag{3}$$

Among them,

$$\sum_i^n \alpha_i = 1 \tag{4}$$

$$\rho = \sum_i^n \alpha_i \rho_i \tag{5}$$

$$\mu = \sum_i^n \alpha_i \mu_i \tag{6}$$

Source terms of the momentum equation due to surface tension and wall adhesion is:

$$F = 2\sigma_{ij}\rho k_i \nabla \alpha_i / (\rho_i + \rho_j) \tag{7}$$

where, ρ is density; μ is dynamic viscosity; α is volume fraction; υ is velocity vector; k is surface curvature.

The forces of liquid, solid, and gas are described by the Gidaspow model, and the inter-gas and liquid forces are described by the schiller-naumann model. At present, the turbulence models that are widely used in numerical simulation are RNG $k-\varepsilon$ model, Realizable $k-\varepsilon$ model and standard $k-\varepsilon$ model. The turbulence model selected for this study is the standard $k-\varepsilon$ model.

2.3. Hydrate slurry physical properties parameter setting

The physical parameters of the hydrate slurry in the numerical simulation were determined based on the experimental data of the high-pressure loop, as shown in Table 1. The viscosity of hydrate slurry was about 0.009–0.02 Pa s (when the hydrate volume fraction is 5%~20%).

(1) Hydrate particle size

Some scholars (Zhao et al., 2016) imported it into FLUENT by writing a user-defined file (UDF), but from the simulation results, the particle size distribution in the center of the pipe was large and the particle size at the pipe wall was small. The conclusion is obviously contrary to the general law. Therefore, this paper will not describe the particle size distribution by means of the particle size model, but to study its influence on the flow field distribution characteristics of hydrate slurry by setting different particle sizes. In general, the solid particle diameter is related to the inner diameter of the pipe by Eq. (8).

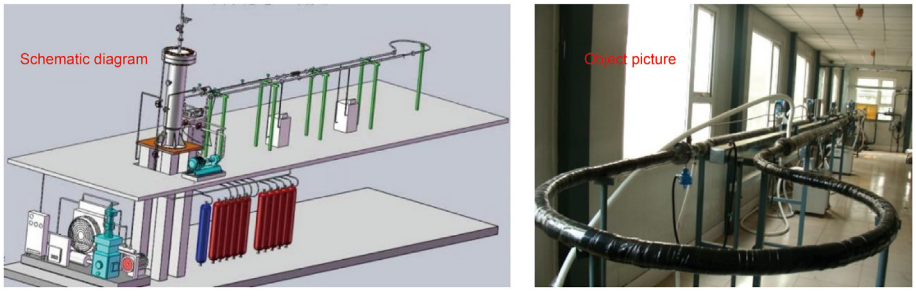

Fig. 2. Schematic diagram of loop model in hydrate slurry experiment.

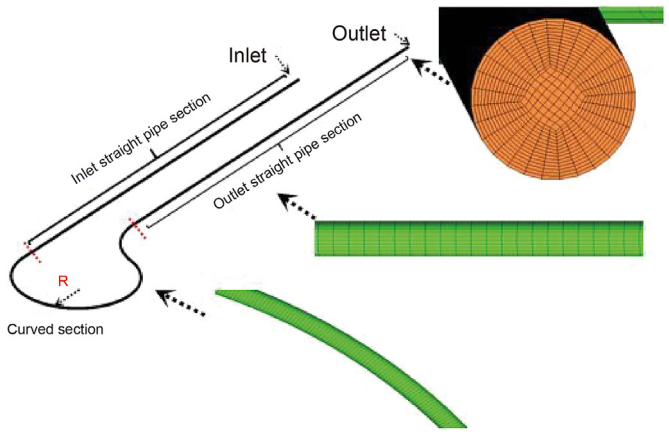

Fig. 3. Mesh generation.

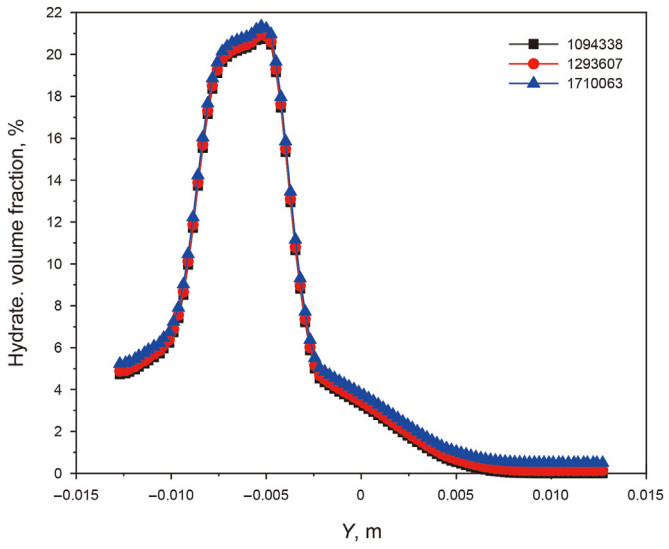

Fig. 4. Grid independence verification.

Table 1
Settings of reference parameters.

parameter	unit	value
Liquid density ρ_l	kg/m^3	1000
Hydrate density ρ_s	kg/m^3	850
Gas density ρ_g	kg/m^3	1.29
Liquid viscosity μ_l	Pa·s	0.0018
Gas viscosity μ_g	Pa·s	1.087×10^{-5}
Hydrate particle size d_s	μm	100~300
Maximum fill rate $\varphi_{s,max}$	%	57
Surface tension coefficient (gas-liquid)	–	0.01
Surface tension coefficient (hydrate-liquid)	–	0.072

$$k=\frac{d}{D} \tag{8}$$

In Eq. (8), k is the proportional variable, which usually does not exceed 0.2. Through microscopic observation instruments such as PVM and FBRM, the initial particle size of hydrate is about 30 μm. When hydrate aggregation occurs, the particle size can reach 200 μm (Lv et al., 2013). According to the model established in this chapter, the pipe diameter is 0.0254 m. Therefore, in this simulation, the hydrate particle size is set as 50–250 μm to study the variation of the multiphase flow characteristics of the hydrate slurry with the particle size.

(2) Packing limit

Regarding the maximum fill rate, researchers have conducted relevant studies (Kitanovski et al., 2005; Kvamme, 2019). The maximum filling rate of hydrate particles is affected by many factors including particle shape, particle size distribution, interaction force, etc. The maximum filling rate of different types of hydrates can be known by consulting the references (Zhao et al., 2016) so far: 52% for ice, 55% for R11 hydrate, 65% for TBAB-A hydrate, and 57% for methane hydrate. Therefore, the maximum filling rate in this chapter is set to 57%.

(3) Hydrate slurry flow velocity

Xia et al. (2002) proposed that there exists a relationship between slip velocity and particle concentration. They calculated that gas hydrate particles have a sedimentation velocity of about 0.35 m/s, while water hydrate particles have a sedimentation velocity of about 0.29 m/s. Therefore, to ensure the safe transportation of hydrate slurry, the particle velocity should be at least greater than 0.29 m/s to ensure that the hydrate particles would not settle. At the same time, based on the experimental data of the loop, the hydrate slurry velocity is higher than 0.5 m/s. Therefore, in this simulation, the flow velocity was set to be 0.5 m/s or more.

2.4. Boundary conditions

The setting of the simulation boundary conditions should be based on the principle that was more conducive to the convergence of the calculation. In this numerical simulation study, considering that the hydrate slurry is an incompressible fluid, the inlet conditions of the pipeline were set as velocity-inlet, the flow direction was perpendicular to the direction of gravity, and the turbulence intensity and hydraulic diameter were calculated and set. The outlet condition of the pipeline was set as the pressure outlet (pressure-outlet), the outlet pressure was 1.8 MPa, the turbulent flow condition and the return hydraulic diameter were the same as those at the inlet, and the wall surface adopted the non-slip wall surface condition.

2.5. Model validation

The multiphase flow experiment under the condition of 5 MPa was carried out on the high-pressure hydrate slurry experimental loop, and the gas-liquid multiphase flow pattern was obtained. The pressure drop value of the flow pattern of the simulated data was compared with the experimental results to test the feasibility of the model. The comparison between the experimental data and the simulated data of the flow pattern and pressure drop factor was shown in Figs. 5 and 6. In addition, the specific results of the pressure drop comparison are shown in Table 2. The flow pattern is almost identical to the experiment. The relative error between the simulated value of the pressure drop factor and the experimental value is less than 15%, which was within the acceptable range. The pressure drop factor in the simulation is not completely equal to the experimental results, which could be attributed to the agglomeration of hydrate particles during the flow process.

3. Three-phase numerical simulation of gas-liquid-solid flow in hydrate slurry

The gas-liquid-solid three-phase flow of hydrate slurry is a common phenomenon in the deep-water hydrate mining process. When the solid hydrate on the seafloor is raised to the sea level, its stable state is destroyed due to the change of the external environment. At this time, the hydrate begins to decompose, releasing gas, and the liquid-solid two-phase flow in the tube becomes the gas-liquid-solid three-phase flow. Based on this, this chapter used the VOF model to simulate the three-phase flow characteristics, flow field distribution, flow pattern transformation, and particle microscopic characteristics of the hydrate slurry in the loop.

3.1. Study on flow characteristics of stratified smooth flow

This section concentrated on the effect of hydrate particle microscopic behavior on stratified smooth flow. Fig. 7 is a cloud map of the distribution of hydrate particle concentrations in the straight pipe section at different times 4.5 m from the entrance. In the initial stage of hydrate slurry flow, the distribution of hydrate in the pipeline was relatively dispersed. As the hydrate slurry flow reached a steady state, the layer of hydrate slowly rose and eventually settled into a stable layer between the gas and liquid phases. The hydrate slurry would continue to flow in the form of a laminar flow.

Fig. 8 showed a cloud map of the distribution of cross-sectional hydrate concentrations at different locations from the inlet. The hydrate slurry in the pipe showed a peaceful delamination. The farther away from the entrance, the greater the maximum number of hydrated object integrals for the cross-section. The maximum volume fraction of the cross-sectional hydrate at 5 m from the inlet can reach 21%. Combined with the hydrate concentration distribution curves of different sections of the straight pipe section in Fig. 9, the closer the section is to the inlet, the higher the hydrate concentration at the bottom of the section. The maximum volume fraction of the section becomes smaller. The maximum volume fraction at the 5 m section position is 1.09 times that at 2 m. The explanation was that with the flow of the slurry, the hydrate solid phase particles gradually aggregated and migrated to the air-water interface under the action of buoyancy.

Fig. 10 is cloud maps and concentration distribution curves of hydrate particle concentrations of different sections of the curved section. The figure shows that when the hydrate slurry flows through the curved section, due to the centrifugal force and additional buoyancy of the slurry, hydrates accumulate on the inner wall of the elbow. Hydrate accumulation leads to an uneven distribution of hydrate concentration in the curved section, causing a shift in the final concentration distribution cloud map and distribution curve.

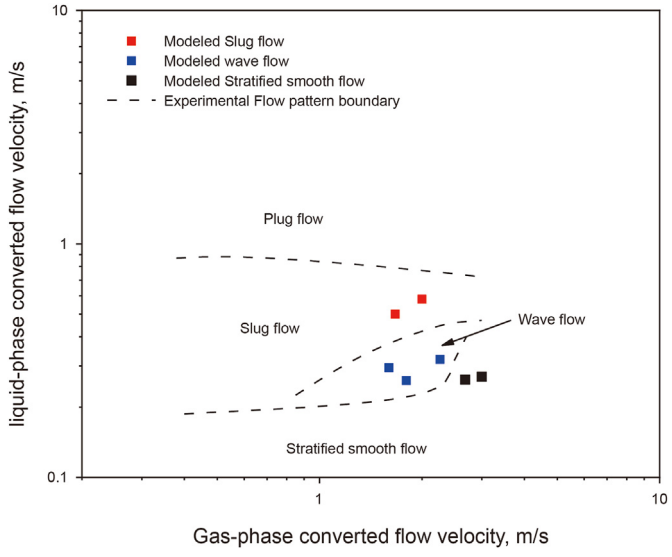

Fig. 5. Comparison of experimental and simulated values of flow pattern of multiphase flow (pressure 5 MPa).

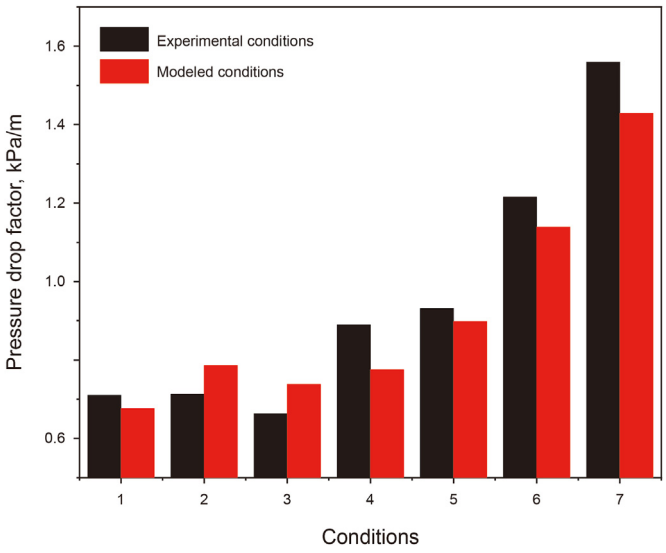

Fig. 6. Comparison of experimental and simulated values of pressure drop factor of pipeline.

3.1.1. Effect of flow velocity

In order to explore the effects of different flow velocities on the flow characteristics and flow field distribution of the stratified smooth flow in the pipeline, different slurry flow velocities were set up for simulation. Fig. 11 showed the cloud map of the particle concentration distribution of cross-sectional hydrate particles at 3.8 m from the inlet at different slurry flow velocities. Owing to the difference in density, the upper part of the pipe section was occupied by the gas phase, and the hydrate concentration is zero. Hydrate particles were mostly concentrated in the middle and lower part of the pipeline, and evenly distributed. As the flow velocity increased, the hydrate layer had a tendency to move to the bottom of the pipeline. The hydrate aggregation layer thickness gradually decreased. This could be explained by the fact that in the middle of the pipe, buoyancy, resistance, and gravity of the hydrate compel the particles to distribute evenly. The increase in flow velocity intensifies the turbulence strength and shear effect of the slurry, and therefore, the hydrate's dispersing ability increases, eventually settling at the bottom of the pipe.

Fig. 12 is a cloud map of the distribution of hydrate particle concentrations in 30° sections of the curved section at different flow velocities. The distribution law of the flow velocity to the particle concentration of the curved pipe section was similar to that of the straight pipe section. However, the hydrate slurry would be affected by centrifugal force when it flowed through the curved section. The centrifugal force shifted the particle concentration distribution and the particles aggregated at the inner wall. Fig. 13(a) and (b) are the cross-sectional concentration distribution curves of 30° and 120° of the curved section. The figure showed that the maximum particle concentration of the section decreased gradually with the increase of the flow velocity. As the flow velocity increased, the maximum volume fraction of hydrate got closer to

Table 2
Comparison between experimental values and simulated values.

Condition	Flow pattern	Liquid flow velocity, kg/h	Experimental pressure drop factor, kPa/m	Modeled pressure drop factor, kPa/m	Relative error, %
1	Stratified smooth flow	300	0.710	0.676	4.79
2	Stratified smooth flow	300	0.713	0.786	10.24
3	Wave flow	300	0.663	0.738	11.31
4	Wave flow	450	0.890	0.775	12.92
5	Wave flow	450	0.931	0.898	3.54
6	Slug flow	750	1.215	1.139	6.26
7	Slug flow	900	1.559	1.429	8.34

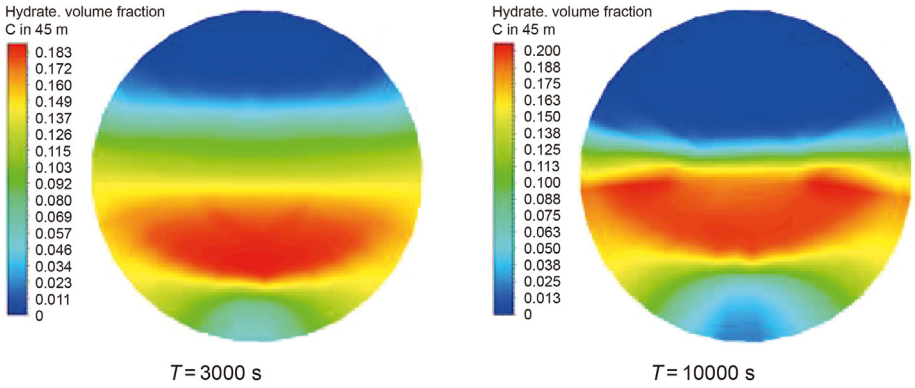

Fig. 7. Cloud diagram of hydrate particle concentration variation in section of straight pipe at different times (inlet straight pipe section 4.5 m).

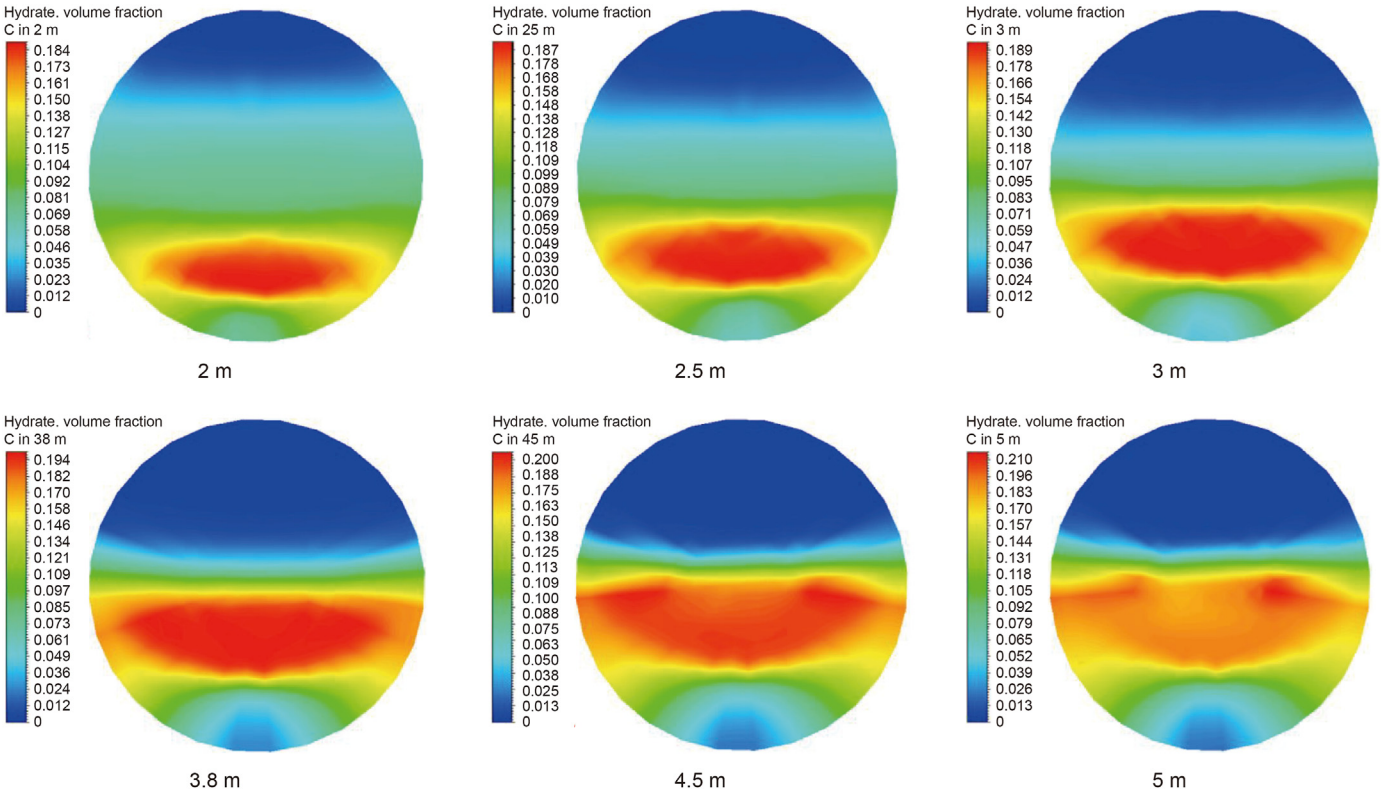

Fig. 8. Hydrate concentration distribution in the inlet straight pipe section.

the bottom of the pipeline.

The preceding studies have shown that the higher the flow velocity, the thinner the liquid holdup of the liquid-solid interface in the tube. A linear fitting method was used in order to determine the correlation between the flow velocity and the thickness of the hydrate moving bed, as shown in Fig. 14. The curve fitting accuracy R^2 was 0.935, which had a fitting high accuracy and met the error requirements. The relationship between the thickness of the

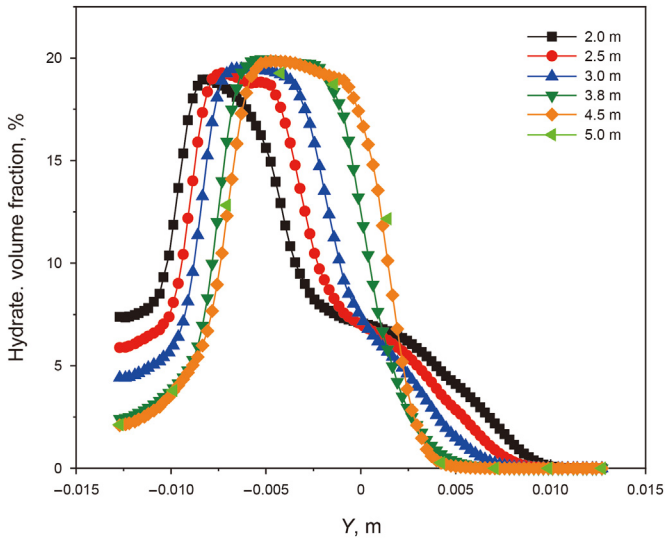

Fig. 9. Hydrate concentration distribution at different sections of inlet straight pipe section.

hydrate moving bed and the flow velocity is obtained, which was expressed by Eq. (9):

$$y_{\text{hydrate}} = 19.243 - 8.795u \tag{9}$$

3.1.2. Effect of particle size of hydrate

Fig. 15 showed the effect of particle size on the distribution of hydrate concentrations in each section of the straight pipe section and the curved section of the loop. The hydrate particles concentration increased in the cross-section of the pipe with the increase of particle size. As shown in Fig. 15(a), the maximum volume fraction for a particle size of 100 μm, at a distance of 2 m from the inlet of the straight pipe section, is 18.96%. Additionally, the maximum volume fraction for 250 μm is 23.75%, which is around 25.26% higher than that for 100 μm. Furthermore, at a distance of 4.5 m from the inlet, the maximum volume fraction for the straight pipe section is 19.84% for a particle size of 100 μm. For the cross-section at 250 μm, the maximum volume fraction is 27.88%, which represents an increase of approximately 40.52%. A similar pattern is observed for the 30° and 90° sections of the curved section, as shown in Fig. 15(b). At the same time, the increase of particle size would also aggravate the inhomogeneity of the hydrate particle concentration distribution in the pipeline section, making the concentration gradient changed larger.

The explanation for the above phenomenon was that the larger the particle size of hydrate particles, the more obvious the collision, coalescence, fragmentation and sedimentation between particles. Researchers (Balakin et al., 2016; Song et al., 2020) generally believed that the coalescence effect was the main factor after the collision of hydrate particles, and the coalescence effect caused the particles to aggregate, which eventually led to an increase in the hydrate volume fraction. Therefore, when the hydrate slurry was transported in the actual mixed pipeline, the particle size should not be too large to control. Larger particle size would lead to an increase in the hydrate volume fraction, which eventually led to flow safety issues.

Fig. 16 is the cloud diagrams of the hydrate concentration distribution at the 30° and 90° sections of the curved section. In the curved section, the larger the particle size of hydrate particles, the more obvious the centrifugal effect, and the more serious the aggregation of hydrate particles on the inner wall of the elbow. This is

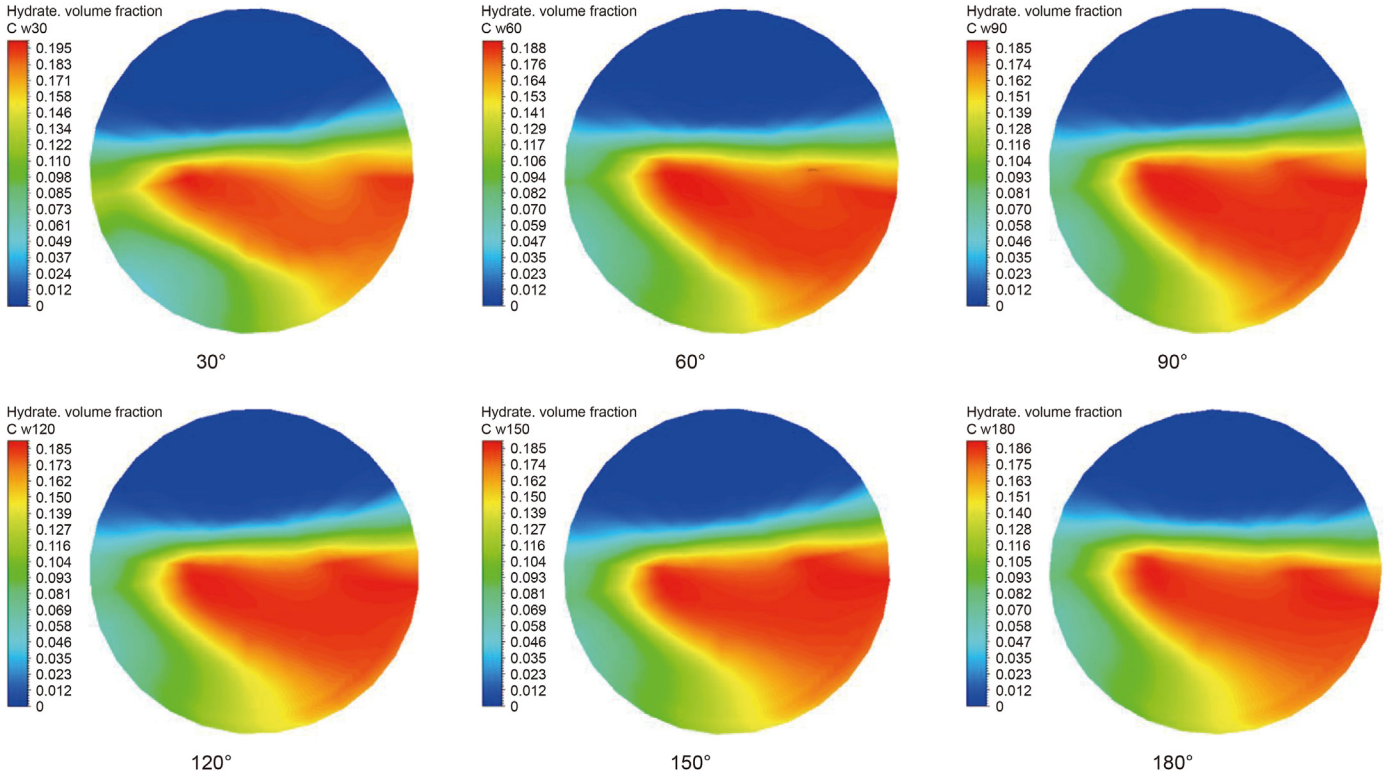

Fig. 10. Hydrate particles concentration distribution at different sections of the curved section.

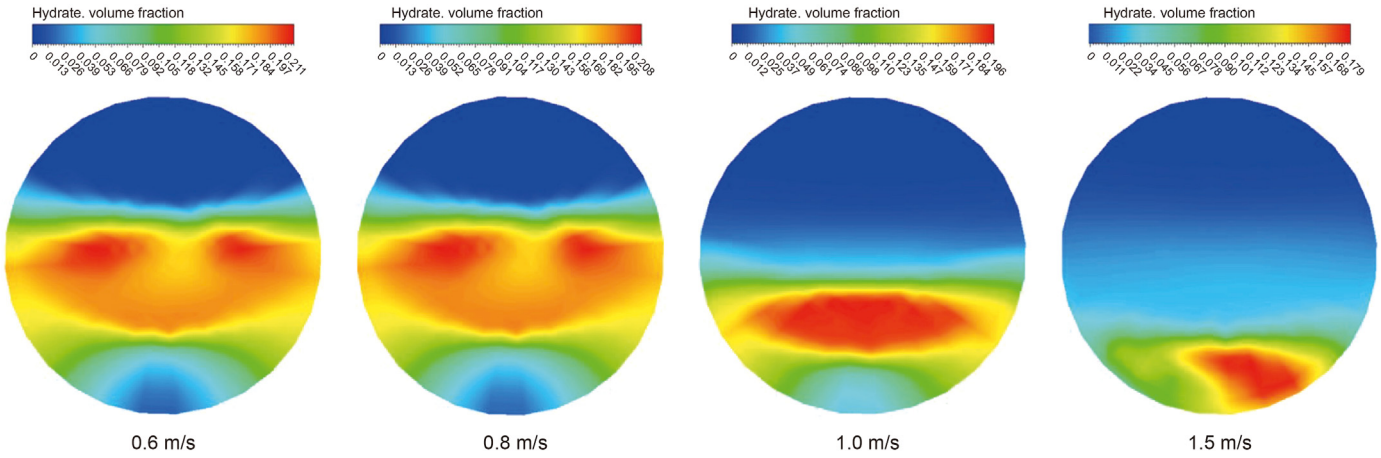

Fig. 11. Influence of velocity on hydrate volume fraction in stratified smooth flow (inlet straight pipe section 3.8 m).

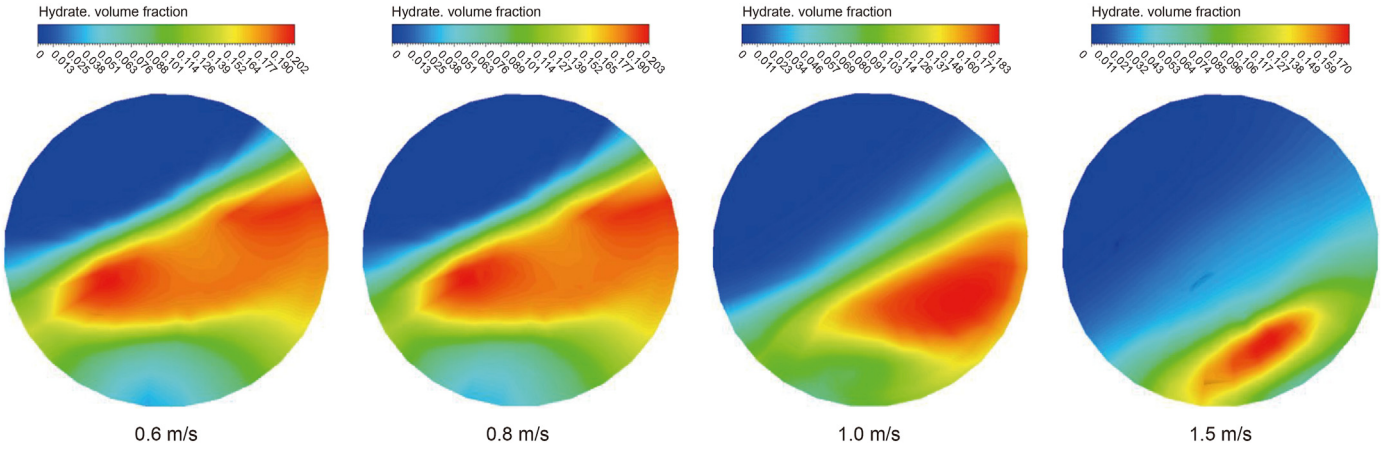

Fig. 12. Influence of velocity on hydrate volume fraction of stratified smooth flow (curved section 30°).

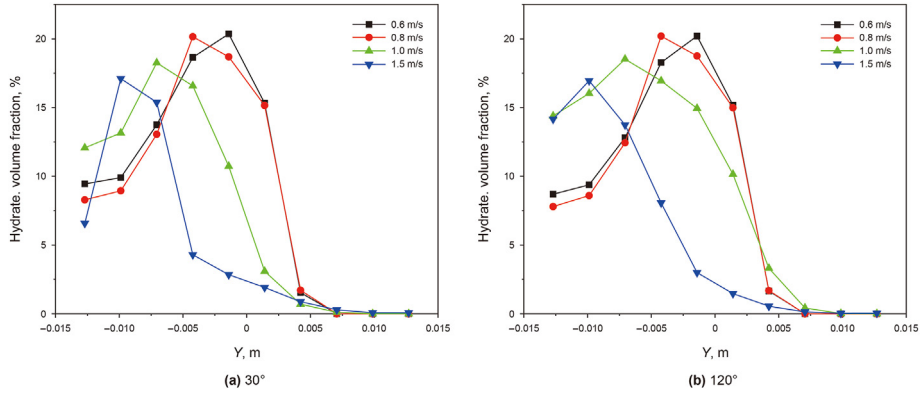

Fig. 13. Influence of velocity on hydrate volume fraction of stratified smooth flow in curved section.

mainly because when the particle size was larger, its mass was also larger, and the inertia of the hydrate becomes larger. This conclusion also indicated that the particle size should not be too large in the actual pipeline system.

Fig. 17 is a cloud map of the hydrate concentration distribution at section 3.8 m away from the outlet. The smaller the particle size is, the easier the hydrate particles were to disperse in the liquid phase, and the more uniform the concentration distribution in the pipeline section. When the particle size increased, a hydrate layer gradually formed in the pipeline. The reason for the above phenomenon is that the particle size increased, the mass and gravity of the particles also increased, and the ability of the particles to follow the flow of the liquid phase became weaker. Hydrates gradually accumulated at the gas-liquid two-phase interface, so the moving bed of hydrates gradually moved upward.

Fig. 18 showed the effect of particle size on the pressure drop

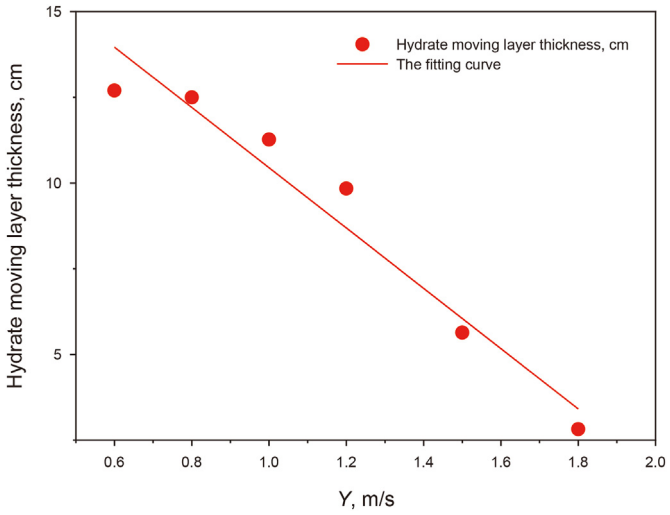

Fig. 14. Relationship between hydrate moving bed thickness and velocity.

gradient across the loop. As can be seen from the figure, as the particle size increased, the pressure drop factor also increased. When the particle size increased from 100 to 250 μm, the pressure drop factor increased by about 3%. There are two main reasons. One is that when the particle size was small, the particle could follow the liquid phase better, and the relative speed between the liquid and the hydrate particles was small, so there were less pressure drop loss. When the particle size increased, the gravity increased, the ability of the particles to follow the liquid phase becomes poor, the relative velocity between the liquid phase and the hydrate increased, and the pressure drop loss increased. On the other hand, the increase in particle size exacerbated collisions between particles, resulting in increased energy loss.

3.1.3. *Effect of hydrate particle density*

In the process of hydrate slurry transport, the change of particle density would also affect the distribution of the flow field in the pipeline and change the flow characteristics of the slurry. Fig. 19 is the cloud map of cross-sectional hydrate concentration distribution at 3.8 m and curved section at different particle densities (850, 1000, 1100 and 1300 kg/m^3) from the inlet 30° and the curved section. Whether it was a straight pipe section or a curved pipe section, as the particle density gradually increased, the hydrate layer gradually moved towards the bottom of the pipe. This was mainly due to the increase in particle density and the increase in gravity.

Fig. 20 showed the effect of hydrate particle density on the pressure drop gradient across the loop. The entire loop was divided

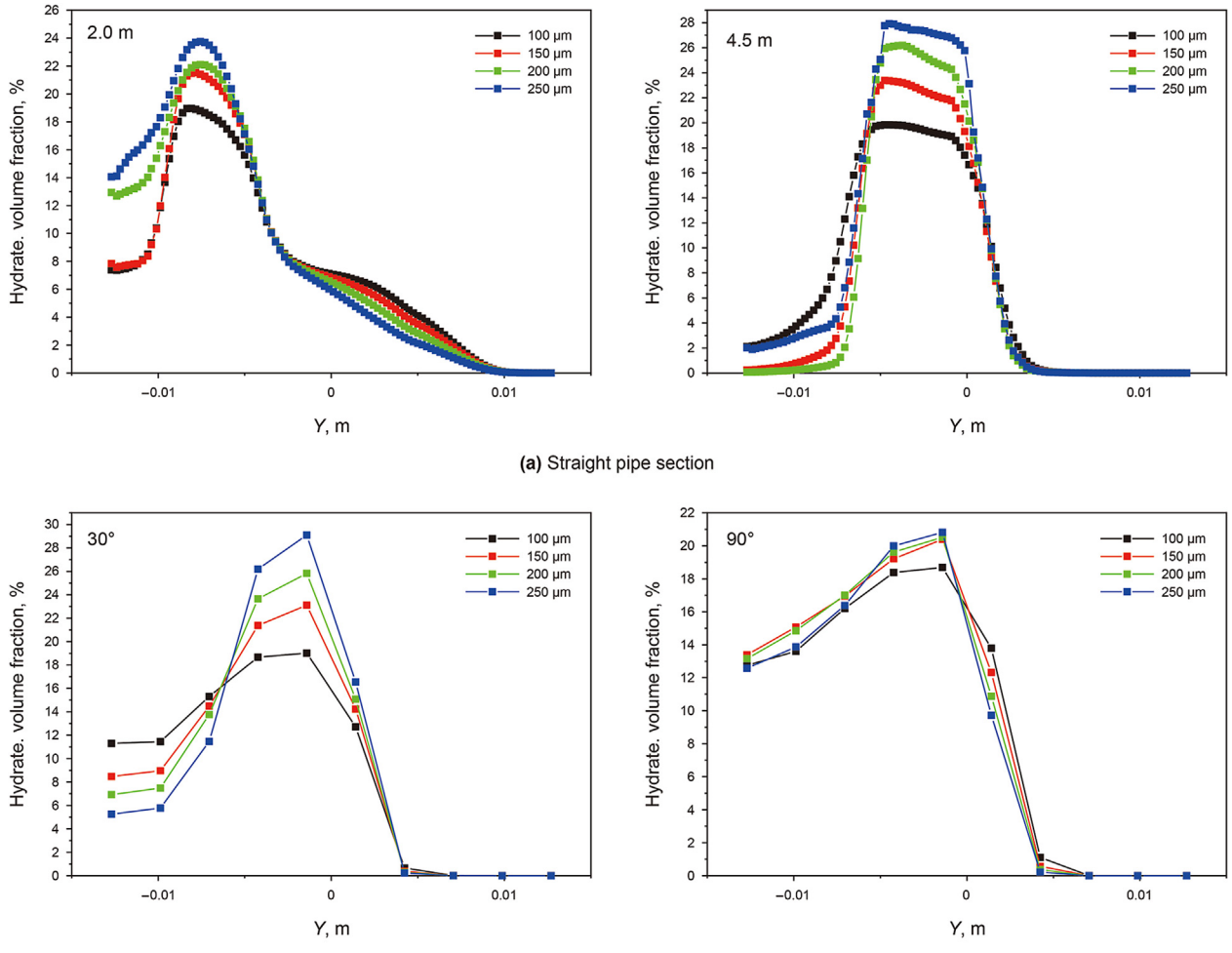

Fig. 15. Concentration distribution of hydrate particles.

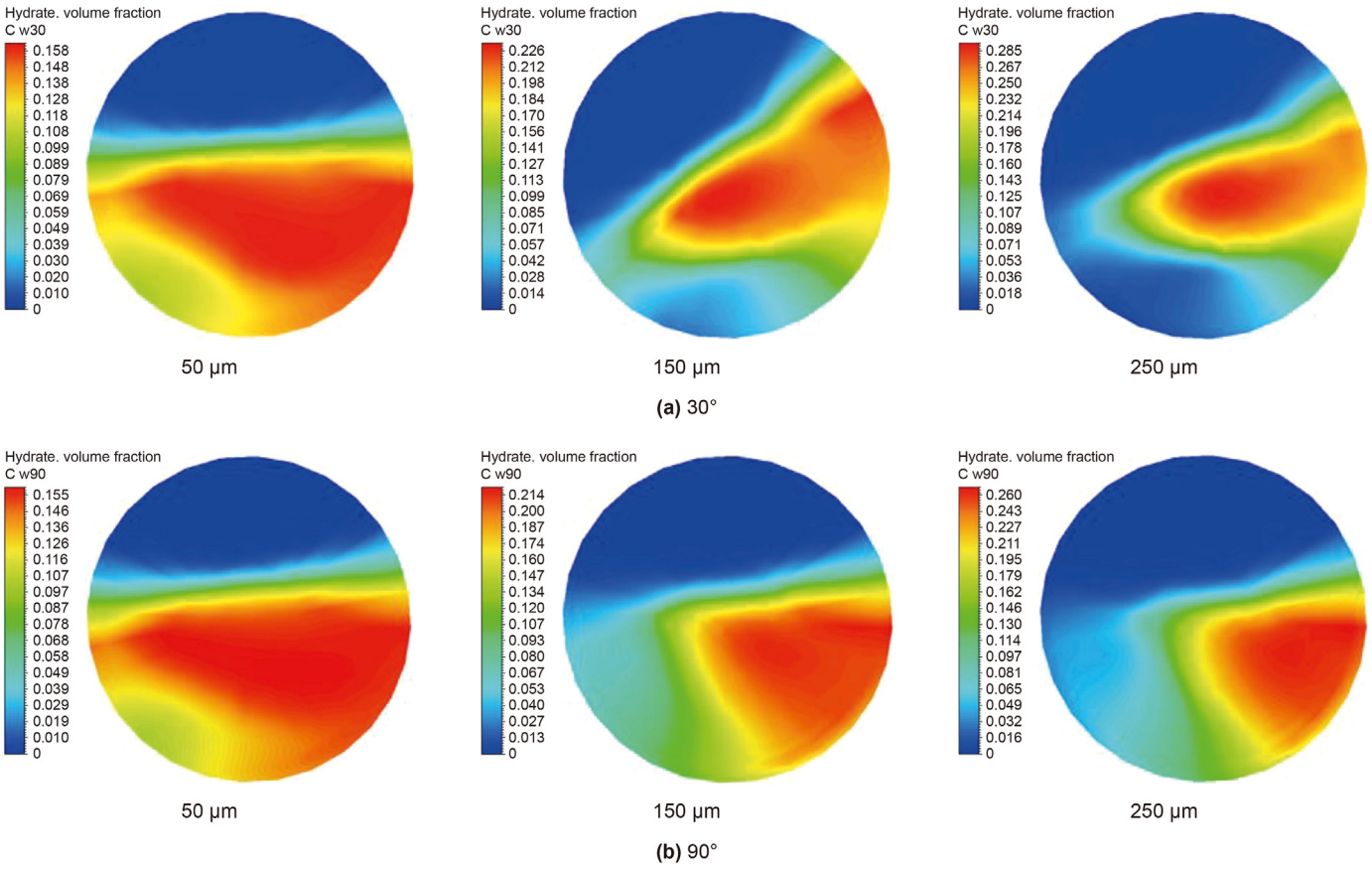

Fig. 16. Variation of particle concentration with particle size in curved section.

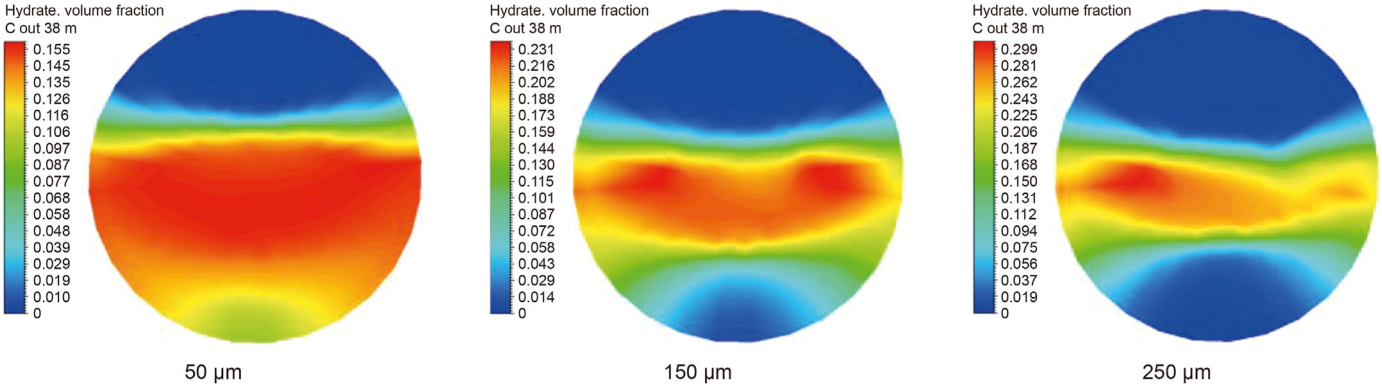

Fig. 17. Variation of hydrate volume fraction with particle size (outlet straight pipe section 3.8 m).

into three parts: the inlet straight pipe section, the curved section, and the outlet straight pipe section. When the hydrate particle density increased from 800 to 1300 kg/m^3, the pressure drop factors of the inlet straight pipe section, the curved section and the outlet straight pipe section increased by 13.21%, 8.42% and 9.57%. On the one hand, the increase in particle density led to an increase in the gravity of the particles, which further led to an increase in the flow resistance of the particles in the slurry. On the other hand, losses due to particle deposition. Therefore, for the actual mixed transmission system, the smaller the particle density, the more conducive to water conservancy transportation.

3.1.4. *Effect of hydrate particle volume fraction*

The hydrate particle volume fraction had an important influence on pipeline transportation flow, pressure loss and transportation efficiency. As shown in Fig. 21, the results showed that no matter in the straight pipe section or the curved pipe section, the particle volume fraction had a great influence on the cross-section hydrate concentration distribution. At 20% volume fraction, the peak value volume fraction was the largest, which was 67% higher than that at 5%. At the same time, the thickness of the hydrate moving bed formed in the middle and lower part of the pipeline was also the thickest. Fig. 22 is the cross-sectional concentration curve distribution, it can be obtained that the gradient of particle concentration increased with the increase of the inlet volume fraction.

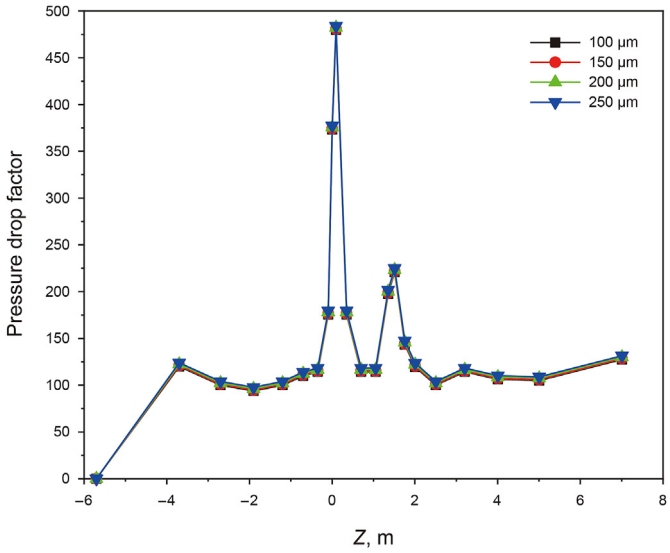

Fig. 18. Influence of hydrate particle sizes on pressure drop.

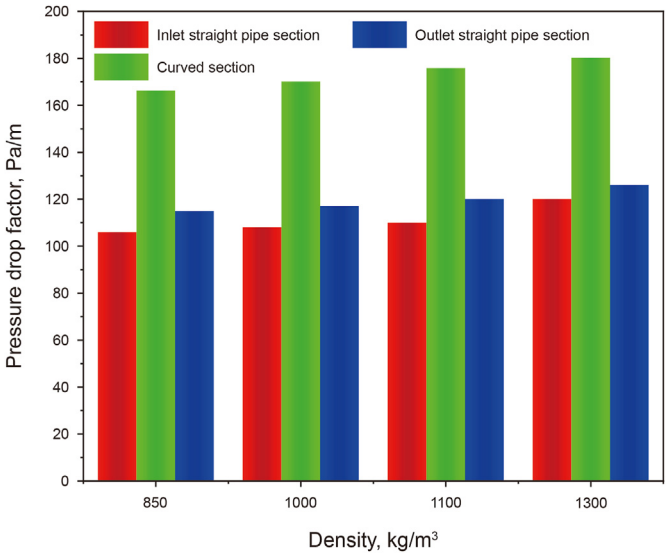

Fig. 20. Influence of hydrate particle density on pressure drop factor.

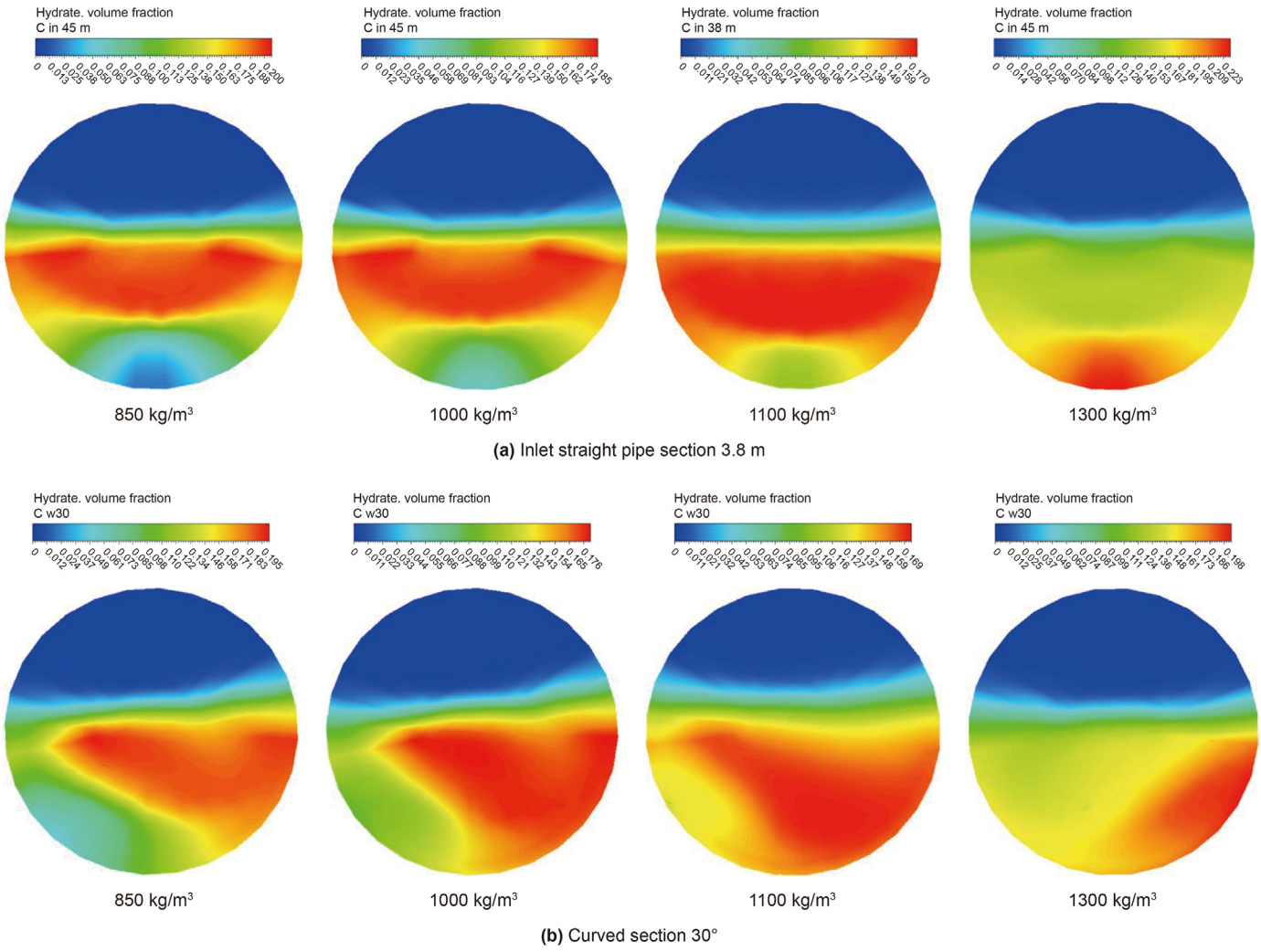

Fig. 19. Distribution cloud of particle concentration at different particle density.

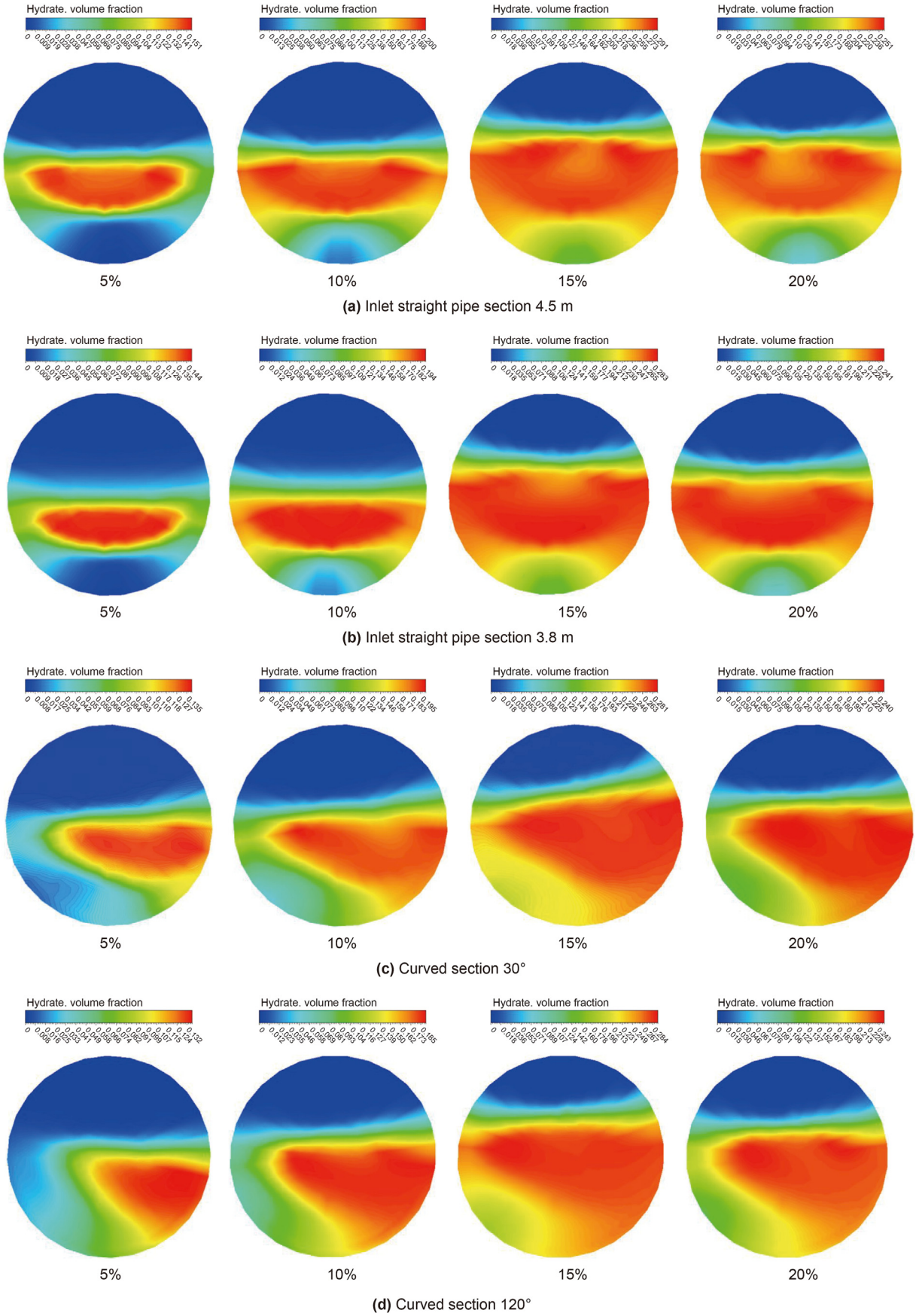

Fig. 21. Hydrate concentration distribution diagram with volume fraction.

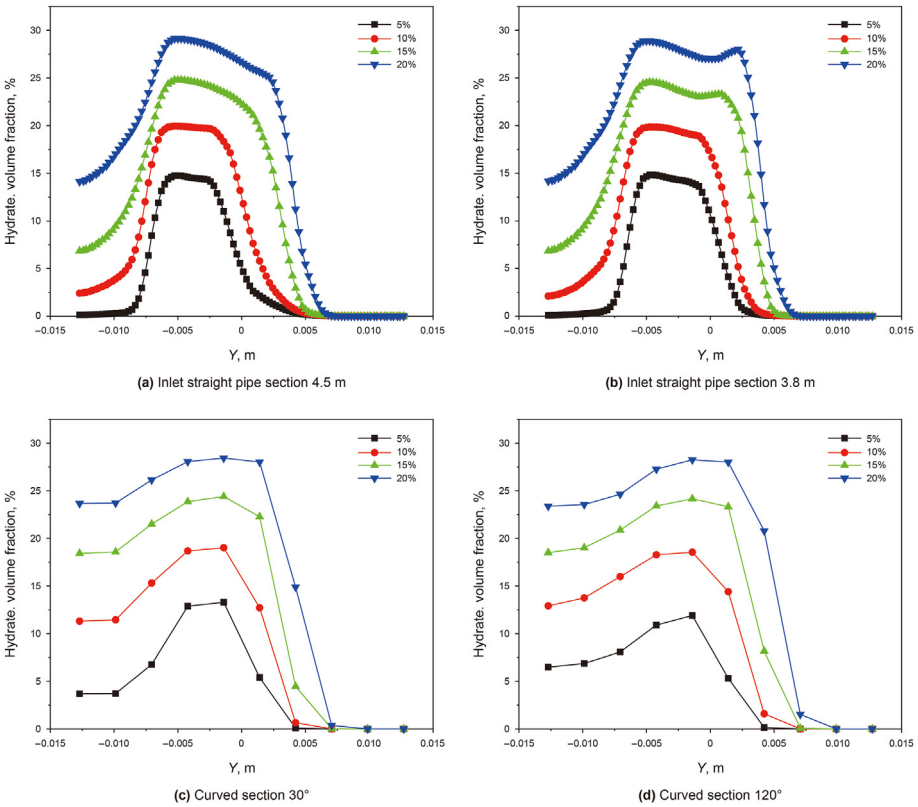

Fig. 22. Variation of particle concentration distribution with volume fraction.

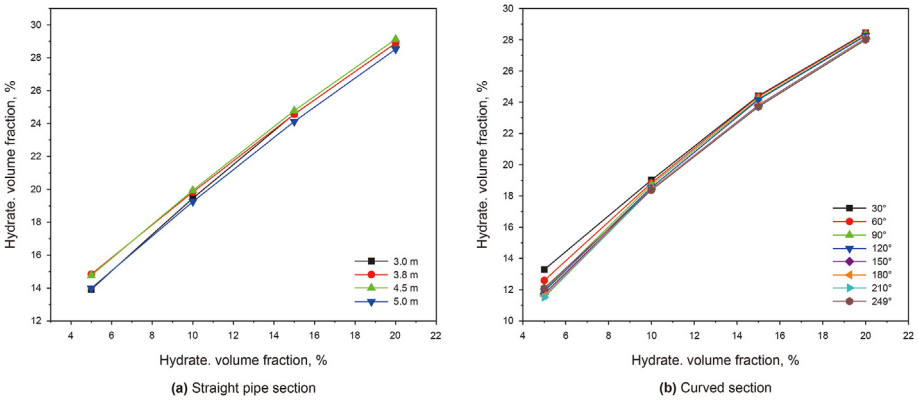

Fig. 23. Relationship between maximum volume fraction and inlet volume fraction.

Fig. 23 showed the relationship between the maximum volume fraction of the section and the inlet volume fraction. In this section, the linear fitting method was adopted, and the relationship between the maximum volume fraction of the section and the inlet volume fraction in the straight pipe section was obtained as shown in Eq. (10):

$$y_{\text{hydrate}} = 10.17069 + 0.95892x \tag{10}$$

The relationship between the two in the curved section was shown in Eq. (11):

$$y_{\text{hydrate}} = 8.58074 + 1.0164x \tag{11}$$

According to the formula, when the hydrate volume fraction reached the maximum filling rate of 57%, the inlet volume fraction of the straight pipe section is 48.835%, and the inlet volume fraction of the curved section is 47.638%. Comparing the inlet volume fraction, it can be seen that hydrate accumulation is more likely to occur in the curved section than in the straight section.

Fig. 24 is the influence curve of the hydrate volume fraction on the pressure drop factor of the entire loop. The larger the volume fraction, the more severe the fluctuation of the pressure drop factor along the line. The maximum value of the pressure drop factor at 20% hydrate volume fraction was about 2.58 times that at 5% volume fraction. The reasons were as follows: the increase of hydrate concentration promoted a higher probability of collision, coalescence and fragmentation between particles. The energy consumption for transporting hydrate slurry increased accordingly, that is, the gradient of pipeline pressure drop increased. Therefore, in order

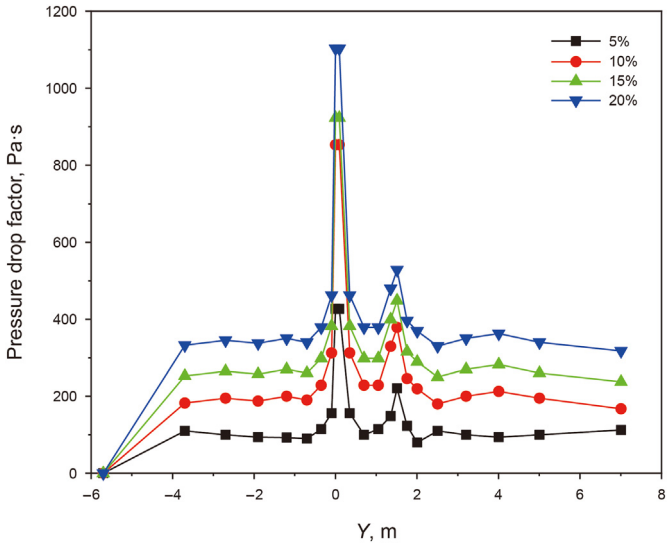

Fig. 24. Changes of the pressure drop factor along the pipeline with the hydrate volume fraction.

to ensure the smooth operation of the pipeline, the concentration of hydrate particles to be transported should not be too large.

3.1.5. Sensitivity analysis of particle concentration distribution in stratified flow

From previous chapters, it can be seen that many factors affected the distribution of hydrate particle concentration. This section would focus on discussing the effects of five factors (flow velocity, particle size, inlet volume fraction, particle density, and liquid viscosity) on the cross-sectional hydrate particle concentration distribution. To judge the stability of hydrate slurry transportation, it is necessary to comprehensively consider the influence of multiple factors. Among them, determining the primary and secondary relationship of the influencing factors was of great significance for guiding the on-site risk prevention and control. This section conducted a sensitivity analysis on the key influencing factors through the orthogonal test method, and each factor took 4 levels. The coefficient n is defined as the evaluation index. The ratio of the maximum cross-sectional concentration to the minimum cross-sectional concentration in the turbulent core region was used to reflect the inhomogeneity of particle distribution. The results were shown in Table 3 and Table 4.

Through the above sensitivity analysis, it could be known that among the five factors, the particle size is the most important factor affecting the distribution of particle concentration, followed by particle density and particle volume fraction. The effects of liquid phase viscosity and slurry flow velocity were minimal. Therefore, the safe delivery of hydrate slurries required close attention to changes in particle size.

3.2. Study on the flow characteristics of wave flow

The simulated slurry velocity for stratified wave flow was 2 m/s. Fig. 25 is a cloud diagram of the concentration distribution of the liquid phase in the pipeline at the inlet straight pipe section

Table 3
Orthogonal test table.

Test number	Velocity, m/s	Liquid viscosity, kg, m·s	Particle size, μm	Particle volume fraction, %	Particle density, kg/m^3	Evaluation indicators, n
1	0.5	0.005	100	5	850	1.0104
2	0.5	0.01	150	10	1000	2.2801
3	0.5	0.015	200	15	1100	1.3338
4	0.5	0.02	250	20	1300	1.2718
5	0.7	0.005	150	15	1300	1.2342
6	0.7	0.01	100	20	1100	1.1109
7	0.7	0.015	250	5	1000	3.0812
8	0.7	0.02	200	10	850	1.1761
9	0.8	0.005	200	20	1000	1.2867
10	0.8	0.01	250	15	850	1.3344
11	0.8	0.015	100	10	1300	1.1490
12	0.8	0.02	150	5	1100	2.1816
13	0.9	0.005	250	10	1100	2.7898
14	0.9	0.01	200	5	1300	2.9866
15	0.9	0.015	150	20	850	1.1304
16	0.9	0.02	100	15	1000	1.1805

Table 4
Results analysis.

Factor	Velocity, m/s	Liquid viscosity, kg/(m·s)	Particle size, μm	Particle volume fraction, %	Particle density, kg/m^3
K_1	5.5861	6.3211	4.4390	8.2598	4.6513
K_2	6.5906	6.7002	6.8263	7.3950	7.8285
K_3	5.9517	6.6944	5.7832	5.0829	7.4063
K_4	7.0873	5.8100	8.4772	4.7880	5.6416
R_j	0.2839	0.2226	1.0096	0.8680	0.7943

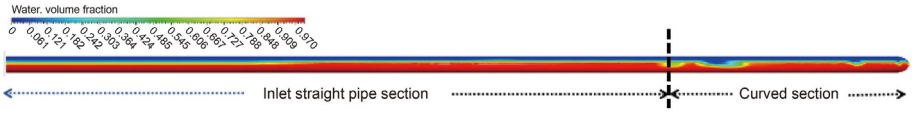

Fig. 25. Concentration distribution of liquid phase during transition from inlet straight pipe section to curved section.

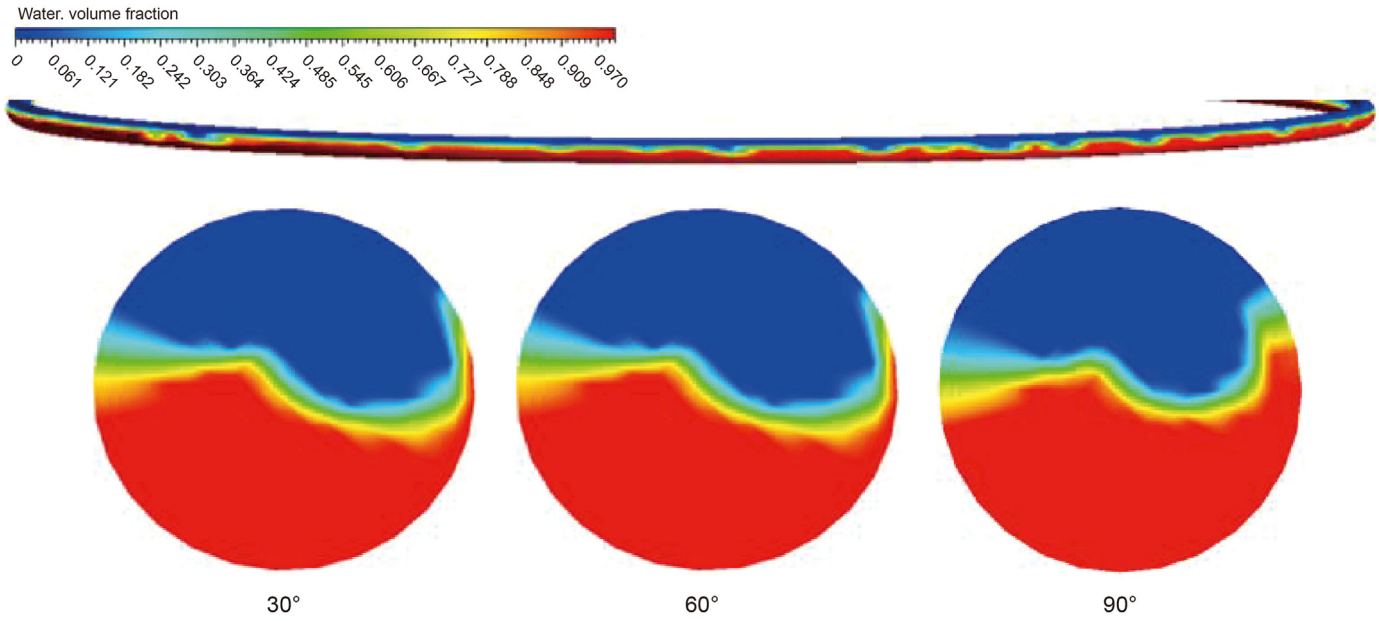

Fig. 26. Concentration distribution of liquid phase in the curved section.

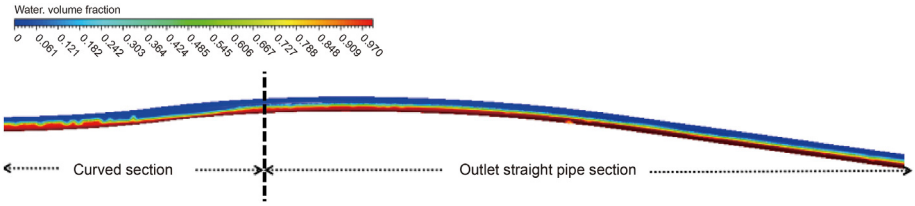

Fig. 27. Liquid concentration distribution of the curved section flowing into the outlet straight section.

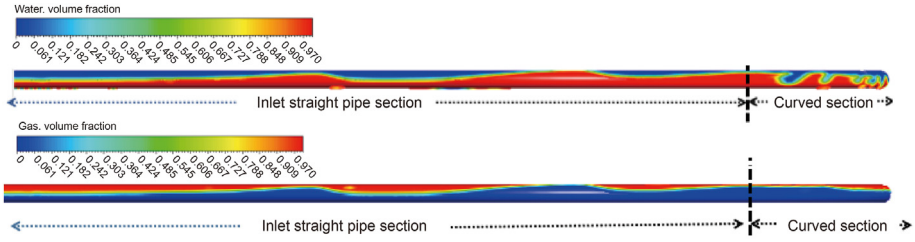

Fig. 28. Liquid and gas phase concentration distribution diagram of the inlet straight pipe section flowing into the curved section.

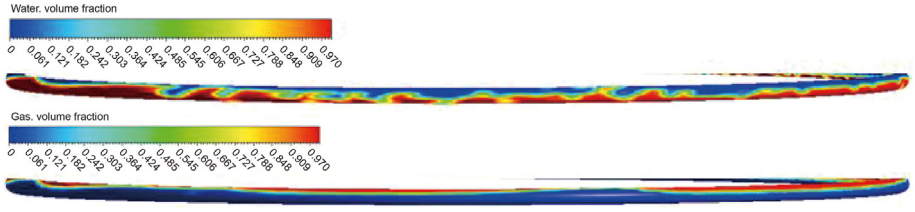

Fig. 29. Liquid and gas phase concentration distribution diagram of the curved section.

transitions to the curved pipe section. In the straight pipe, the hydrate slurry maintained a good stratified flow. When the hydrate slurry flowed from the straight pipe to the curved pipe, the disturbance of the gas, liquid and solid three-phase interface caused the wave flow to appear. The reason for the change of flow pattern could be explained as follows: in the straight pipe section, the flow direction of the slurry remained unchanged, the collision and aggregation effects between particles were quite weak, and the slurry maintained a stratified smooth flow motion. However, when the slurry flowed to the curved section, the flow direction changed,

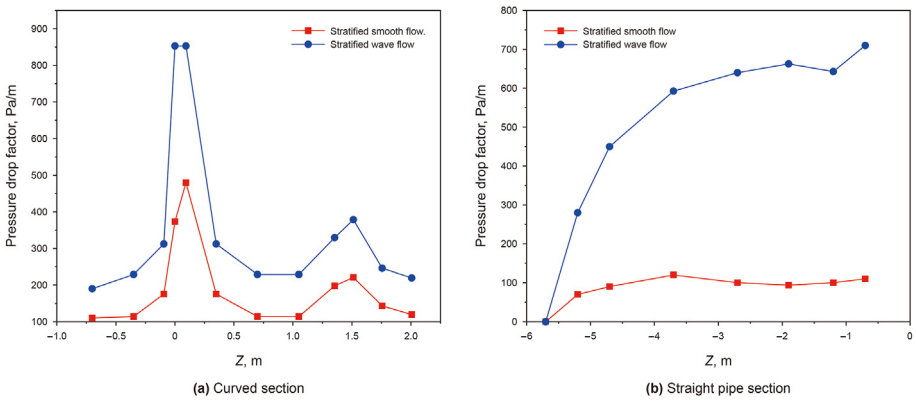

Fig. 30. Comparison of pressure drop factors between stratified smooth flow and wave flow in the same position.

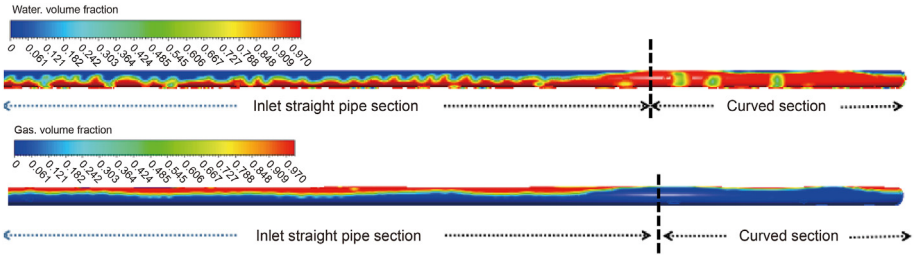

Fig. 31. Liquid and gas concentration distribution of the inlet straight pipe section flowing into the curved section.

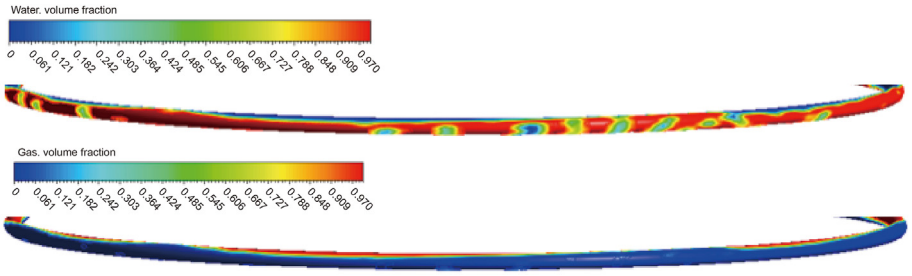

Fig. 32. Liquid and gas concentration distribution of the curved section.

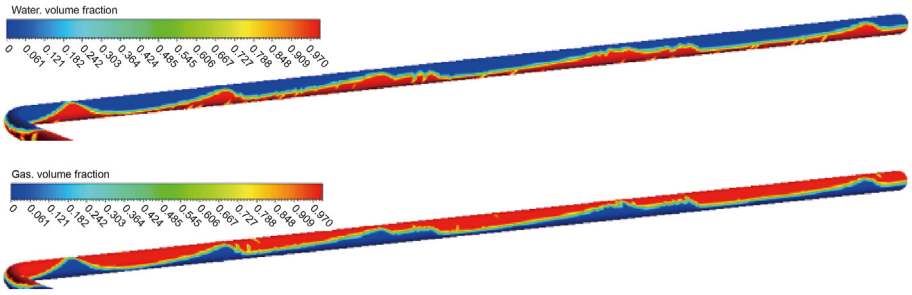

Fig. 33. Liquid and gas concentration distribution of the outlet straight pipe section.

the hydrate particles collision and coalescence were intensified. In addition, the hydrate slurry was subjected to centrifugal force when flowing through the elbow, which eventually led to the flow pattern from stratified smooth flow transitions to wavy flow. Fig. 26 showed that the hydrate slurry kept the wave flow after entering the curved section, and there was obvious disturbance at the phase interface.

Fig. 27 showed a cloud diagram of the liquid phase concentration distribution when the hydrate slurry flows out of the elbow and into the outlet straight pipe section. In the figure, the flow pattern of hydrate slurry gradually transitioned from wavy flow to stratified smooth flow. The main reason for the above phenomenon

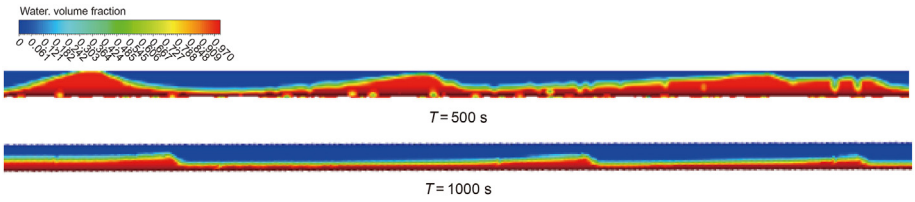

Fig. 34. Liquid phase distribution diagram at different time at slug flow position.

was that after the slurry flowed out of the curved section into the outlet straight pipe, the flow field direction changed and the particle concentration changed. The change of particle concentration affected the viscosity and flow pattern distribution of the whole slurry, so the flow pattern changed from wavy flow to stratified smooth flow.

When the slurry flow rate is increased to 3 m/s, as shown in Fig. 28. The inlet straight pipe section changes from a layered flow to a pronounced wave flow. Near the elbow, due to the increase in the gas phase flow rate, the pressure above the liquid phase decreases, and the liquid phase reaches the top of the tube, and a small segment plug flow occurs. After the hydrate slurry flowed into the elbow, the flow pattern was transformed into a wave flow with strong fluctuations, as shown in Fig. 29. It could be seen that by increasing the slurry flow velocity, the hydrate slurry flow pattern could be transformed from stratified smooth flow to wave flow.

As shown in Fig. 30, the pressure drop fluctuation of wave flow was larger than that of stratified smooth flow. As shown in Fig. 30(a), at the 90° position of the curved section, the maximum pressure drop factor of the wave flow reached 853.04 Pa/m, while the pressure drop factor of the stratified smooth flow here was 479.84 Pa/m. The pressure drop factor of wave flow was about 1.78 times that of stratified smooth flow. As shown in Fig. 30(b), in the straight pipe section at the inlet, the pressure drop factor of the wave flow could reach 7.07 times that of the stratified smooth flow at the same position. The main reason for the above phenomenon is that the disturbance and instability of the wave flow aggravated the flow loss of the slurry, resulting in an increase in the pressure drop gradient. Therefore, in the actual mixed pipeline transportation of slurry, in order to ensure the safety of transportation, it should be ensured that the hydrate slurry was transported in a stratified smooth flow.

3.3. Study on flow characteristics of slug flow

This section will focus on the effect of particle micro-behavior on slug flow patterns. Adjusted the slurry velocity to 4 m/s on the basis of wave flow. As shown in Fig. 31, the straight pipe section at the inlet presented a violent wavy flow. The hydrate slurry entered the curved section, the liquid phase was blown up by the gas with high flow velocity. The liquid-phase reached the top of the pipe, and the entire pipe section was filled with liquid to form a liquid plug. In the entire curved section, as shown in Fig. 32, the hydrate slurry kept flowing in the slug flow, and the liquid phase almost filled the entire curved section. In the outlet straight pipe section, as shown in Fig. 33, the slug was weakened and a long wave flow appeared. The reason for the slug flow could be summed up as follows: due to the Bernoulli effect. The increase in gas flow velocity caused the pressure at the peak of the liquid wave to decrease. Under the action of the higher pressure around the peak, the height of the liquid wave rose, a slug flow was formed.

Fig. 34 is a cloud diagram of the liquid phase concentration distribution at the slug position of the outlet straight pipe section. The figure showed that the slug flow intensity gradually decreased with time. At T=500 s, the hydrate particles promoted the formation of strong slug flow with low aggregation effect. The viscosity of the hydrate slurry increased gradually as the particle agglomeration in the flow region of the hydrate slurry increased and the hydrate particles entrained in the gas phase enter the slug body. The increase in viscosity increased the adhesion between the pipe wall and the fluid. At the same time, the increase of the average density of the hydrate slurry also increased the gravity of the slurry. Both of these effects would weaken and inhibit slug flow. Therefore, when T=1000 s, the flow pattern was no longer slug flow. From the simulation results of the slug flow, it could be seen that the presence of hydrate particles would weaken the slug flow and inhibit its formation.

3.3.1. Effect of particle volume fraction

Considered that when the slurry flow velocity was 3 m/s, a tiny slug flow had already appeared in the transition area from the straight pipe to the curved pipe. Therefore, on the basis of 3 m/s, this section adjusted the hydrate particles volume fraction, and observed the effect of the change of volume fraction on the slug flow pattern. Fig. 35(a)–(c) showed the distribution of liquid phase concentration in the transition zone from the inlet straight pipe to the curved pipe, the curved pipe section, and the outlet straight pipe section. The figure showed that below 10% concentration, the number, length and height of slug bodies all increased to varying degrees with the increase of the volume fraction. This is mainly because of the increase of the hydrate volume fraction. The liquid phase velocity decreased and the gas phase slip velocity increased sharply, resulting in an increase in the pressure difference above the wave. At the same time, more hydrate particles in the liquid phase reduced the average density of the liquid phase, which reduced the wave gravitational potential energy, resulting in the transition from the liquid phase to wave or slug flow. Above 10% concentration, with the increase of hydrate particle volume fraction, the slug tendency gradually decreased, and the height as well as number of slug bodies decreased. This could be explained that when there were more hydrate particles in the slurry, the content of hydrate particles in the formed slug body was high, thereby increasing the gravity of the slug body. The slurry viscosity also increased meanwhile with the increase of particle concentration, which eventually resulted in a gradual decrease in the trend of segment congestion.

3.3.2. The effect of particle density

Fig. 36(a) and (b) are the changes of the slug flow pattern of the curved pipe section and outlet straight pipe section under different particle densities. The figure showed that with the increase of particle density, the trend of slug flow in the curved section and the outlet straight pipe section did not change significantly. The overall trend of slug flow decreased with the increase of particle density in a small range, and this rule was most obvious when the curved section flowed into the exit straight section. The foremost reason is that the particle density increased, resulting in a larger weight and

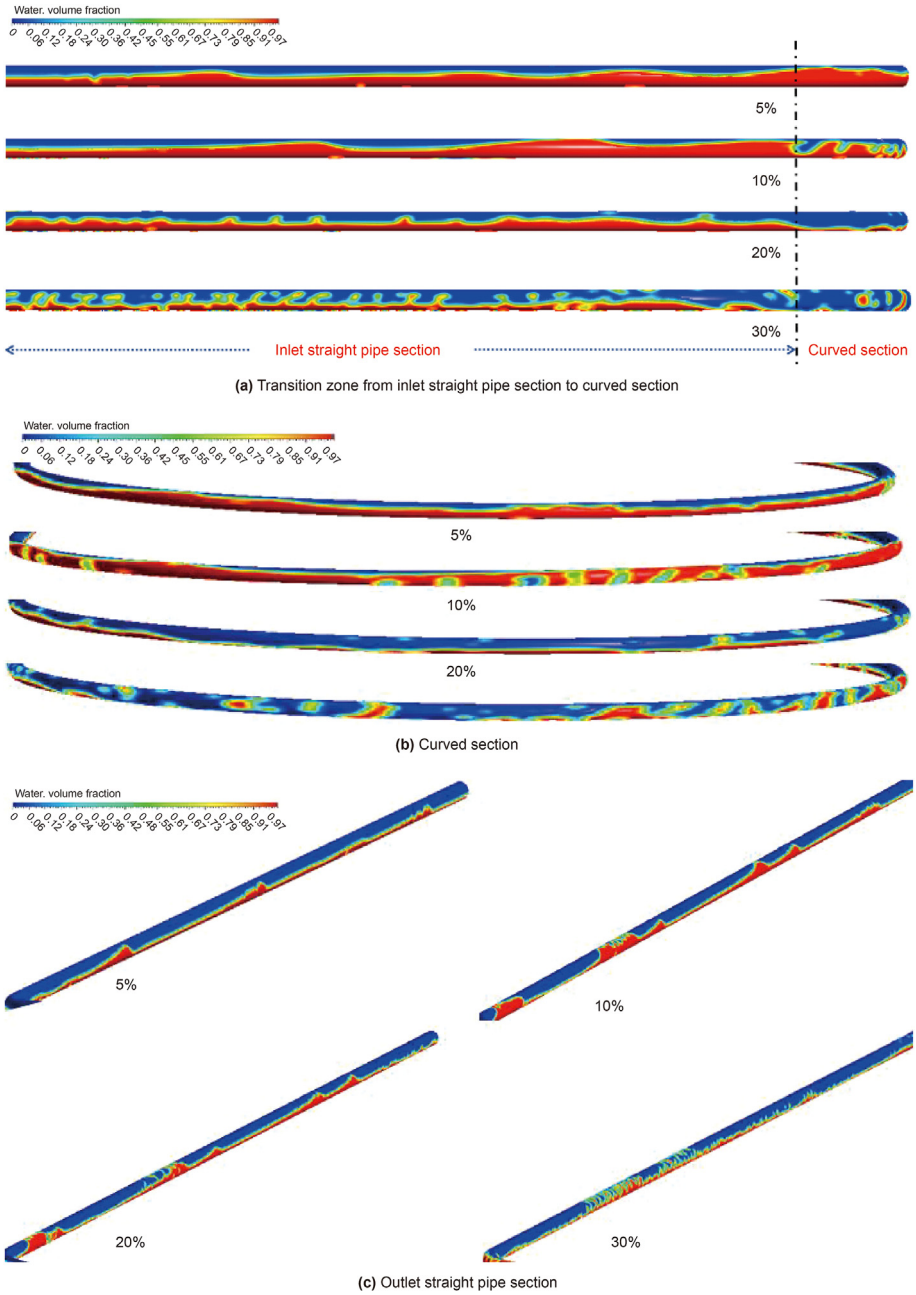

Fig. 35. Liquid concentration distribution diagram.

gravity. Under the action of increasing gravity, the liquid phase height reduced. In addition, the change in the direction of the flow field led to a change in the distribution of particle concentration, which intensified the aggregation and deposition effect of particles. Particle agglomeration weakened the slug flow tendency.

3.3.3. Effect of liquid phase viscosity

Figs. 37 and 38 are the cloud diagrams of the concentration distribution of the liquid phase and the gas phase under different liquid viscosities. The figure showed that with the increase of the liquid viscosity, the slug flow trend gradually weakened. When the liquid viscosity reached as high as 0.02 kg/(m·s), the slug flow no longer appeared in the outlet straight pipe section. This is mainly because the increase in the viscosity of the liquid phase led to a decrease in the flow velocity of the slurry and an increase in the apparent flow velocity of the gas phase. As the gas flow velocity increased, the ability to carry the liquid phase increased, so the height of the liquid phase decreased slightly, and the slug tendency gradually weakened.

3.3.4. Comparison of slug flow pressure drop and layered flow smooth flow

Slug flow is often accompanied by huge disturbances in the flow process. Fig. 39 showed a comparison of the pressure drop factor of the curved section and the outlet straight pipe section. The figure showed that in the curved section and the outlet straight pipe section, the pressure drop factor of the slug flow and the stratified smooth flow showed a huge difference. As shown in Fig. 39(a), the maximum value of the pressure drop factor reached 5011 Pa/m in the curved section, which is about 487.46% higher than 853 Pa/m of

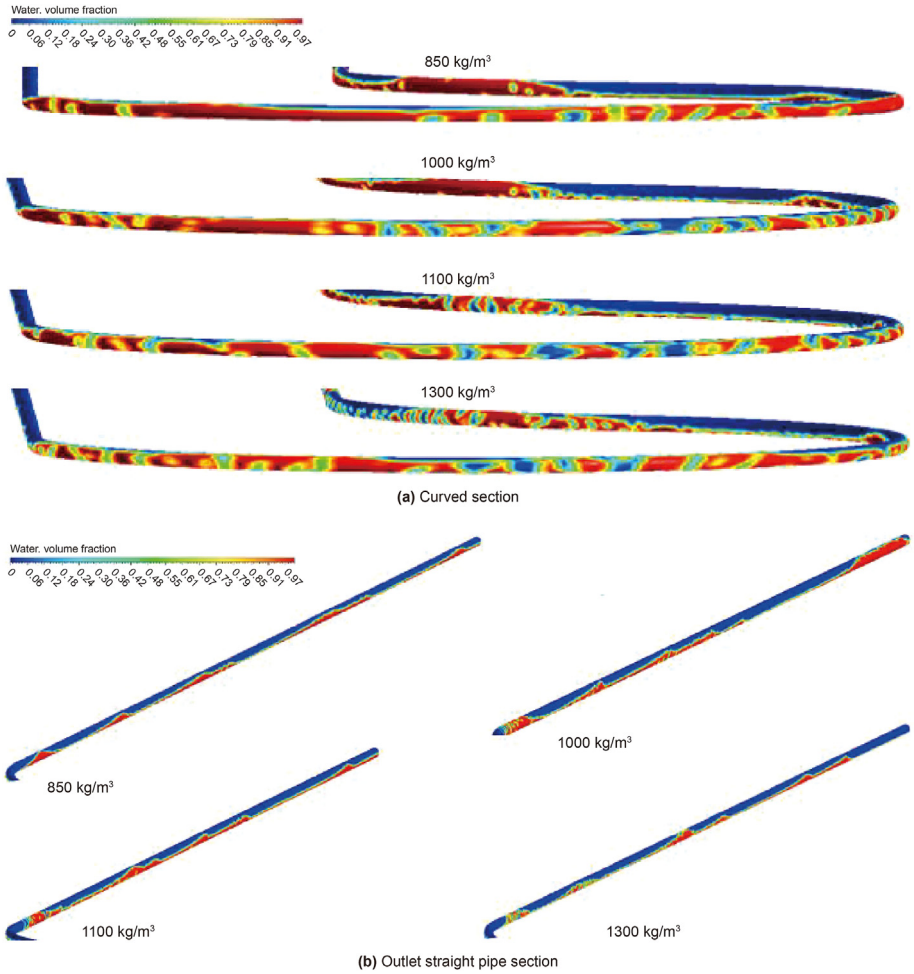

Fig. 36. Liquid concentration distribution under different particle density.

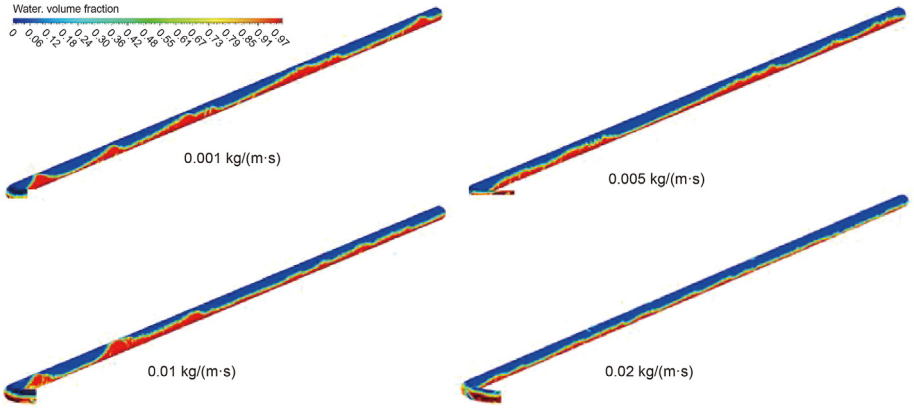

Fig. 37. Liquid concentration distribution under different liquid viscosity (outlet straight pipe 3.8 m).

the stratified smooth flow. As shown in Fig. 39(b), in the outlet straight pipe section, the maximum value of the pressure drop factor reached 2280 Pa/m, which is 20.73 times that of the stratified smooth flow pressure drop factor of 110 Pa/m. It is concluded that when the slurry flows in slug flow, a huge pressure drop gradient would appear in the pipeline, which seriously threatened the safe operation of the pipeline and equipment. At the same time, according to the flow pattern simulation results of the hydrate slurry in the ring channel, the place where the flow of the section plug is prone to occur at the location of the inflow into the curved section and the outflow of the curved section. Therefore, in the actual mixed pipeline hydrate slurry transport process, it is necessary to understand the mechanism of slug flow generation and preventive measures. Special attention deserved the area

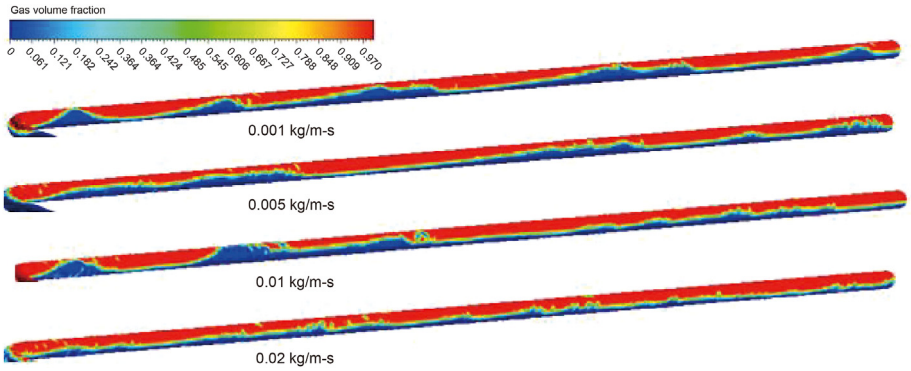

Fig. 38. Gas concentration distribution under different liquid viscosity (outlet straight pipe 3.8 m).

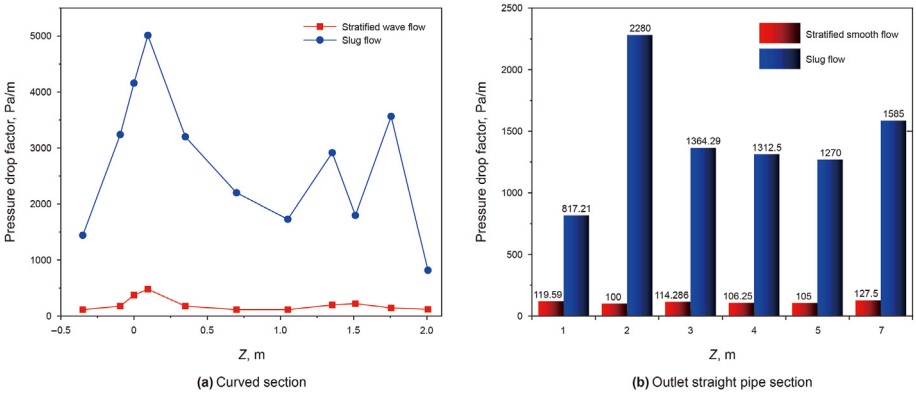

Fig. 39. Comparison of pressure drop factors of stratified smooth flow and slug flow in the same position.

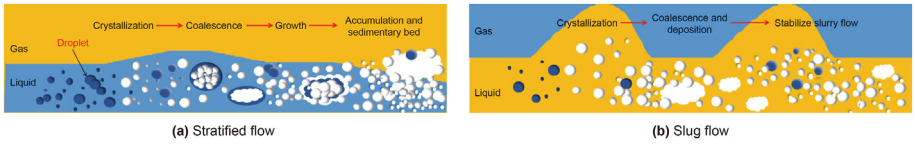

Fig. 40. Schematic diagram of pipeline blocking mechanism under stratified flow and slug flow.

where the direction of the flow field changed.

3.4. Clogging mechanism of different flow patterns

Fig. 40(a) is a blocking mechanism diagram of a stratified flow, where hydrate particles were formed at the gas-liquid interface or on the surface of a water droplet, and then gradually formed large aggregates through a coalescing effect. The viscosity of the slurry gradually increased, resulting in a gradual decrease in the flow velocity. The ability of particles to follow the liquid phase gradually weakened, followed by deposition and eventually blocking the pipeline.

Fig. 40(b) is a blocking mechanism diagram of the slug flow, and unlike the stratified flow, there is no obvious hydrate growth process in the slug flow. Hydrate particles formed on the surface of the water droplet and at the gas-liquid-tube wall interface. Hydrate particles would undergo violent coalescence and sedimentation effects. However, due to the huge disturbance and strong shearing action of the slug flow, the large hydrate aggregates were pulverized into small hydrate particles, so the pipeline was not prone to blockage.

4. Conclusions

(1) The influence of key parameters such as flow velocity, particle size, particle density, and particle volume fraction on the distribution of stratified flow fields was analyzed. The quantitative relationship between the following variable groups was obtained by using the linear fitting method: flow velocity and thickness of hydrate moving bed, maximum volume fraction and inlet volume fraction. The corresponding fitting formula was obtained; it proved to be more predictable. The pressure drop factor along the line increased with an increase in particle size, particle density, and hydrate volume fraction. According to the orthogonal test method, the particle size was found to have the most significant impact on the uneven distribution of particle concentration in the stratified flow.

(2) Increasing the slurry flow rate can realize the transformation of the hydrate slurry from stratified smooth flow to wave flow. The slurry flow velocity was increased to 2 m/s, and the slurry showed a wave flow only the curved section. When the velocity continued to increase to 3 m/s, the inlet straight pipe section changes from a stratified smooth flow to a

pronounced wave flow. It was concluded that increasing the slurry flow velocity could realize the transformation of the hydrate slurry from stratified smooth flow to wave flow. The pressure drop of the wave flow fluctuated more than in the stratified smooth flow. At the 90° position of the curved section, the pressure drop factor of the wave flow was about 1.78 times that of the stratified smooth flow. In the inlet straight pipe section, the pressure drop factor of the wave flow could reach 7.07 times that of the stratified smooth flow at the same position.

(3) The slug flow replaced the wave flow when the slurry flow rate is increased to 4 m/s. The presence of hydrate particles weakened the slug flow and inhibited its formation. Below the particle concentration of 10%, the segment congestion flow trend would be strengthened as the volume fraction of hydrate particles increased. At particle concentrations above 10%, the situation was completely opposite, with the increase of the volume fraction of hydrate particles, the segment congestion flow trend would weaken. Similarly, the slug flow trend also weakened with the increase of particle density and liquid phase viscosity. In the curved section, the maximum pressure drop factor of the slug flow is about 487.46% higher than the stratified flow. In the outlet straight pipe section, the maximum pressure drop factor is 20.73 times than that of the stratified flow. The blocking mechanism of different flow types was analyzed, which provided reasonable suggestions for the safe transportation of deep-water mixed transmission system.

Declaration of competing interest

The authors declare that they have no known competing financial interests or personal relationships that could have appeared to influence the work reported in this paper.

Acknowledgement

This work was supported by the National Natural Science Foundation of China (Grant No.52274061 & 52004039 & 51974037), China Postdoctoral Science Foundation (Grant No.2023T160717 & 2021M693908), The major project of universities affiliated to Jiangsu Province basic science (natural science) research (Grant No.21KJA440001), Jiangsu Qinglan Project, Changzhou Longcheng Talent Plan-Youth Science and Technology Talent Recruitment Project. Numerical computations were performed on Hefei advanced computing center.

References

Bai, D., Chen, G., Zhang, X., et al., 2015. How properties of solid surfaces modulate the nucleation of gas hydrate. Sci. Rep. 5 (1), 12747. https://doi.org/10.1038/srep12747.

Balakin, B.V., Lo, S., Kosinski, P., et al., 2016. Modelling agglomeration and deposition of gas hydrates in industrial pipelines with combined CFD-PBM technique. Chem. Eng. Sci. 153, 45–57. https://doi.org/10.1016/j.ces.2016.07.010.

Ding, L., Shi, B., Liu, Y., et al., 2019. Rheology of natural gas hydrate slurry: effect of hydrate agglomeration and deposition. Fuel 239, 126–137. https://doi.org/10.1016/j.fuel.2018.10.110.

Ding, L., Shi, B., Lv, X., et al., 2017. Hydrate formation and plugging mechanisms in different gas–liquid flow patterns. Ind. Eng. Chem. Res. 56 (14), 4173–4184. https://doi.org/10.1021/acs.iecr.6b02717.

Duan, X., Shi, B., Wang, J., et al., 2021. Simulation of the hydrate blockage process in a water-dominated system via the CFD-DEM method. J. Nat. Gas Sci. Eng. 96, 104241. https://doi.org/10.1016/j.jngse.2021.104241.

Gong, J., Shi, B., Chen, Y., et al., 2020. Submarine multiphase pipeline transport containing natural gas hydrate and its plugging risk prevention and control. Nat. Gas. Ind. 40, 133–142. https://doi.org/10.3787/j.issn.1000-0976.2020.12.015.

Joshi, S.V., Grasso, G.A., Lafond, P.G., et al., 2013. Experimental flowloop investigations of gas hydrate formation in high water cut systems. Chem. Eng. Sci. 97, 198–209. https://doi.org/10.1016/j.ces.2013.04.019.

Kitanovski, A., Vuarnoz, D., Ata-Caesar, D., et al., 2005. The fluid dynamics of ice slurry. Int. J. Refrig. 28 (1), 37–50. https://doi.org/10.1016/j.ijrefrig.2004.07.010.

Koh, C.A., Sum, A.K., Sloan, E.D., 2012. State of the art: natural gas hydrates as a natural resource. Engineering 8, 132–138. https://doi.org/10.1016/j.jngse.2012.01.005.

Kvamme, B., 2019. Environmentally friendly production of methane from natural gas hydrate using carbon dioxide. Sustainability 11, 1964. https://doi.org/10.3390/su11071964.

Lv, X., Shi, B., Wang, Y., Gong, J., 2013. Study on gas hydrate formation and hydrate slurry flow in a multiphase transportation system. Energy Fuel. 27, 7294–7302. https://doi.org/10.1021/ef401648r.

Lv, X., Zhang, J., Liu, Y., et al., 2022. Simulation study of natural gas hydrate slurry flow characteristics in a high-pressure flow loop. Fuel 316, 123332. https://doi.org/10.1016/j.fuel.2022.123332.

Lv, X.F., Zuo, J.W., Liu, Y., et al., 2019. Experimental study of growth kinetics of CO_2 hydrates and multiphase flow properties of slurries in high pressure flow systems. RSC Adv. 9 (56), 32873–32888. https://doi.org/10.1039/c9ra06445a.

Paz, P., Netto, T.A., 2020. On the rheological properties of thermodynamic hydrate inhibitors used in offshore oil and gas production. J. Mar. Sci. Eng. 8 (11). https://doi.org/10.3390/jmse8110878.

Peng, B.Z., Chen, J., Sun, C.Y., et al., 2012. Flow characteristics and morphology of hydrate slurry formed from (natural gas+diesel oil/condensate oil+water) system containing anti-agglomerant. Chem. Eng. Sci. 84, 333–344. https://doi.org/10.1016/j.ces.2012.08.030.

Shen, X.D., Hou, G.D., Ding, J.X., et al., 2018. Flow characteristics of methane hydrate slurry in the transition region in a high-pressure flow loop. J. Nat. Gas Sci. Eng. 55, 64–73. https://doi.org/10.1016/j.jngse.2018.04.023.

Shi, B.H., Chai, S., Wang, L.Y., et al., 2016. Viscosity investigation of natural gas hydrate slurries with anti-agglomerants additives. Fuel 185, 323–338. https://doi.org/10.1016/j.fuel.2016.07.113.

Shi, B., Song, S., Chen, Y., et al., 2021. Status of natural gas hydrate flow assurance research in China: a review. Energy Fuel. 35 (5), 3611–3658. https://doi.org/10.1021/acs.energyfuels.0c04209.

Sloan, D., Creek, J., Sum, A.K., 2011. Chapter two - where and how are hydrate plugs formed? In: Sloan, D., et al. (Eds.), Natural Gas Hydrates in Flow Assurance. Gulf Professional Publishing, Boston, pp. 13–36.

Sloan, E.D., Koh, C.A., 2007. Clathrate Hydrates of Natural Gases. CRC press. https://doi.org/10.1201/9781420008494.

Song, G., Li, Y., Wang, W., et al., 2018. Numerical simulation of hydrate slurry flow behavior in oil-water systems based on hydrate agglomeration modelling. J. Petrol. Sci. Eng. 169, 393–404. https://doi.org/10.1016/j.petrol.2018.05.073.

Song, G., Li, Y., Wang, W., Shi, Z., 2020. Numerical simulation of hydrate particle size distribution and hydrate particle bedding in pipeline flowing systems. J. Dispersion Sci. Technol. 41 (7), 1051–1064. https://doi.org/10.1080/01932691.2019.1614043.

Stoporev, A.S., Svarovskaya, L.I., Strelets, L.A., Altunina, L.K., Manakov, A.Y., 2018. Effect of reactor wall material on the nucleation of methane hydrate in water-in-oil emulsions. Mendeleev Commun. 28 (3), 343–344. https://doi.org/10.1016/j.mencom.2018.05.039.

Sun, B., Fu, W., Wang, Z., et al., 2019. Characterizing the rheology of methane hydrate slurry in a horizontal water-continuous system. SPE J. 25. https://doi.org/10.2118/195586-PA.

Umuteme, O.M., Zahidul Islam, S., Hossain, M., Karnik, A., 2022. An improved computational fluid dynamics (CFD) model for predicting hydrate deposition rate and wall shear stress in offshore gas-dominated pipeline. J. Nat. Gas Sci. Eng. 107, 104800. https://doi.org/10.1016/j.jngse.2022.104800.

Wang, W., Fan, S., Liang, D., Li, Y., 2010. Experimental study on flow characteristics of tetrahydrofuran hydrate slurry in pipelines. J. Nat. Gas Chem. 19 (3), 318–322. https://doi.org/10.1016/S1003-9953(09)60072-4.

Wang, Y., Fan, S., Lang, X., 2019. Reviews of gas hydrate inhibitors in gas-dominant pipelines and application of kinetic hydrate inhibitors in China. Chin. J. Chem. Eng. 27 (9), 2118–2132. https://doi.org/10.1016/j.cjche.2019.02.023.

Xia, J., Ni, J., Huang, J., 2002. Retention effect of coarse granular materials in vertical pipe flow. Min. Metall. Eng. (3), 37–40 (in Chinese).

Xu, Z., Sun, Q., Gao, J., et al., 2021. Experiment and model investigation of D-sorbitol as a thermodynamic hydrate inhibitor for methane and carbon dioxide hydrates. J. Nat. Gas Sci. Eng. 90, 103927. https://doi.org/10.1016/j.jngse.2021.103927.

Yang, M., Zhao, J., Zheng, J., et al., 2019. Hydrate reformation characteristics in natural gas hydrate dissociation process: a review. Appl. Energy 256, 113878. https://doi.org/10.1016/j.apenergy.2019.113878.

Zhang, L., Sun, L., Lu, Y., et al., 2021. Molecular dynamics simulation and in-situ MRI observation of organic exclusion during CO_2 hydrate growth. Chem. Phys. Lett. 764, 138287. https://doi.org/10.1016/j.cplett.2020.138287.

Zhao, P., Wang, W., Li, Y., et al., 2016. Numerical model of hydrated slurry flow in pipelines. Oil Gas Storage Transp. 35 (3), 272–277 (in Chinese).

Zhong, Y., Qing, Y., Yang, H., et al., 2021. Numerical simulation of slurry flow characteristics of hydrate in pipelines based on fluent. Nat. Gas. Chem. Ind. 46 (4), 126–132. https://kns.cnki.net/kcms/detail/51.1336.TQ.20210622.0848.012.html (in Chinese).